An Off-Grid Photovoltaic Power System with MPPT Charge Controller

By

Owen G. Massey

Henry L. Peterson

Evan P. Sacker

Initial Design Report for EECE 472, Senior Design, Winter 2021

February 16, 2021

Table of Contents

1 Introduction **4**
1.1 Problem 5
1.2 Proposed Solution 5

2 Background **6**
2.1 Solar Panels 6
2.2 DC-DC Converters 7
2.3 Battery Charging 8
2.4 Maximum Power Point Tracking 9
2.4.1 Perturb and Observe Algorithm 10
2.5 Similar Research 15
2.6 Ethical Concerns 16
2.7 Contribution to Society 17

3 Design **18**
3.1 System Diagram 18
3.2 MPPT DC-DC Converter 18
3.3 DC-DC Regulator Converter 20
3.4 MOSFET Driver Circuit 21
3.5 Battery Storage And Battery Charging IC Circuit 22
3.6 Control Unit 24
3.7 Bill of Materials and Cost Considerations 25

4 Simulation Results **26**
4.1 Simulation with Resistive Load 26
4.2 Simulation with Battery Load 33

5 Completed Test Results and Discussion **38**

6 Future Work **44**
6.1 System Testing Plan 44
6.2 Work Schedule 45
6.3 Potential Problems 45

7 Works Cited **46**

8 Appendix **49**

1 Introduction

Much of the world lives without access to electricity or reliable electricity infrastructure. Many of these people would benefit from distributed energy technologies if they were offered at an affordable price. Solar photovoltaics (PV) continue to become cheaper and more efficient, yet these resources remain too expensive for the impoverished communities that would benefit the most from them. For off-grid generation to be a feasible option for many people, they must maximize their investment returns by purchasing only the most efficient systems. This is not only true for low cost applications, it is also applicable to any solar PV application restricted in available space for mounting panels or in regions with limited solar irradiance. The purpose of our project is to demonstrate one method to address this issue by increasing solar PV efficiency and value. This report details the design and implementation plan for a small-scale off-grid photovoltaic battery charging system with PV power optimization.

1.1 Problem

Solar panels have a varying internal resistance as a function of solar irradiance [1]. Without intelligent control, the power generated by the solar panel will not be optimized; maximum power transfer is achieved by matching the impedance of the source and load.

1.2 Proposed Solution

In order to provide the highest electrical efficiency, solar photovoltaics require maximum power point tracking (MPPT), an algorithm which alters converter characteristics, including average equivalent impedance, to maximize the power generated by the solar panels. We plan to demonstrate this optimization algorithm in a solar PV battery charging power system. Our system will consist of one solar panel, two DC-DC converters, a lead acid battery, a lead acid battery charging IC, and one Arduino Uno microcontroller. Our simplified system will represent the core of many high efficiency solar PV power systems.

2 Background

2.1 Solar Panels

As the world's energy systems transition away from fossil fuel based power sources, photovoltaic solar energy generation has an expanding role in providing electricity for both on-grid and off-grid applications. Solar is an ideal choice for off-grid applications due to its relatively low upfront and maintenance costs [2]. A solar panel converts solar radiation from the sun into direct current electricity by taking advantage of layering silicon based semiconductors and the photoelectric effect. When a photon of light strikes the silicon lattice of a solar cell, an electron-hole pair is created, the p-n junction separates the electron and the corresponding hole, creating a differential area of charge and therefore a DC voltage across the cell [3]. Monocrystalline silicon is used in 95% of solar panels on the market as its crystal lattice most efficiently converts photon input into current [4].

Solar panels have a power rating that is determined under standard test conditions (STC) which are defined as 1,000 Watts/m² at 77 degrees Fahrenheit. A peak sun hour is defined as an hour in which average solar radiation is at or above standard test condition solar irradiance [3]. This means that a given panel will theoretically output its given power rating for that hour, disregarding various practical inefficiencies. For a given latitude and time of year, the number of peak sun hours (T_{sun}) is constant. Given the number of peak sun hours and the rated power (P_{rated}) of the array, you can calculate the array's energy output (E_{out}) as shown by Equation 1.

$$E_{out} = T_{sun} \times P_{rated} \quad (1)$$

The main challenge facing photovoltaic solar power is the natural resource's inherent intermittency. The sun is sometimes covered by clouds, and at night there is no sun at all. Therefore, a solar system must be integrated with a sufficiently sized battery bank to allow for continuous power supply to an off-grid system. A day of autonomy (DOA) is described as a day's worth of usable electrical energy stored in the system's battery bank to continuously supply power, assuming there is zero solar energy input. Designing a system with more days of autonomy will make it more reliable in poor weather conditions, but will also require a larger battery bank capacity which increases system cost and physical size [5].

2.2 DC-DC Converters

A DC-DC converter controls the flow of power between two different direct current devices. Commonly, these kinds of converters are used to power voltage dependent loads, charge and discharge batteries, and increase system efficiency through maximum power point tracking. A DC-DC converter is the DC equivalent to an AC transformer, and provides an efficient way to transform DC voltage levels. The three most basic types of DC-DC converters are the buck converter, which lowers the input voltage, the boost converter, which raises the input voltage, and the buck-boost converter, which is capable of both raising or lowering the input voltage. All of these topologies use diodes, inductors, capacitors, and switching transistors to create an average output voltage that is higher (boosting) or lower (bucking) than its input.

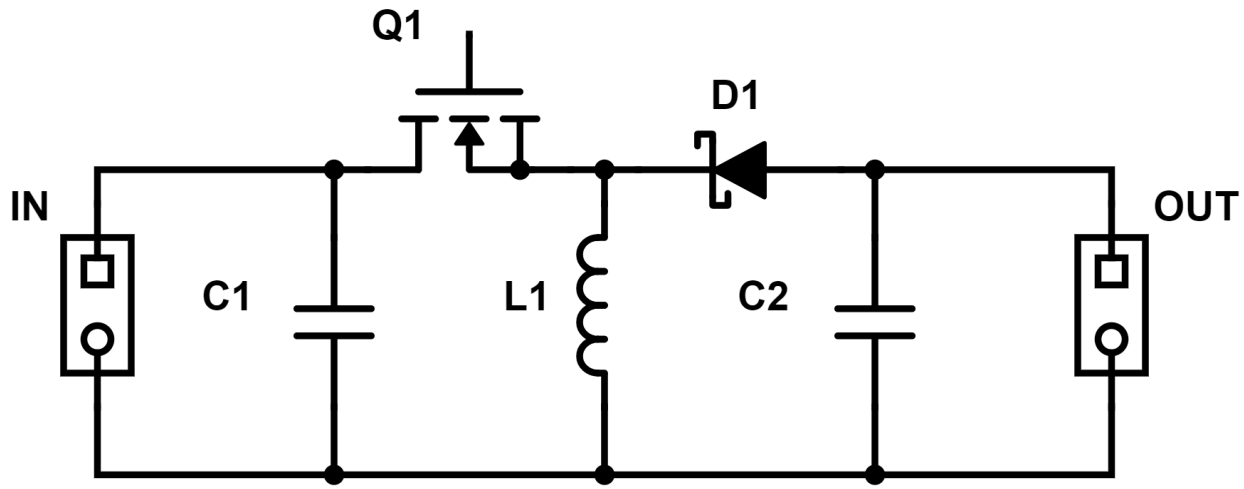

Figure 1: Basic Buck-Boost DC-DC Converter Model.

The buck-boost converter, shown in Figure 1, steps up or down an input DC voltage by utilizing a controllable switch such as an N-Channel MOSFET (Q1), a diode (D1), an inductor (L1), and a capacitor (C2). The input capacitor (C1) acts as a low pass filter for noise presented at the power source. When the gate signal to Q1 is high (closed circuit) D1 is reverse biased (open circuit), current flows through L1 and energy storage in the form of a magnetic field is developed.

When the gate signal to Q1 is low (open circuit) the magnetic field around L1 collapses and current discharges across the load through the diode, which is now forward biased (closed circuit). This in turn develops an electric field across C2, which further discharges across the load on the following gate pulse iteration. This mechanism allows the stepping up or down of voltage from the input to the output. By varying the duty cycle (D), which is the percentage of the time that the gate signal is high, the output voltage (V_{out}) can be varied from zero to theoretically infinity as D sweeps from zero to one. This relationship is shown in Equation 2.

$$V_{out} = V_{in} \frac{-D}{1-D} \quad (2)$$

In practice, buck-boost converters are usually not operated in the upper or lower range of the duty cycle to avoid damage to the components. It is also important to note that, unlike the buck and boost topologies, the buck-boost converter creates an output with an inverted voltage compared to the input. There are more complex topologies that circumvent this problem, but for our purposes this is not a significant deterrent to this topology. To evaluate the performance of these converters, the voltage and current ripples, or unwanted AC harmonic, at L1 and C2 can be calculated and measured [6].

2.3 Battery Charging

Off-grid systems usually require a method of energy storage to combat intermittency of renewable sources and chemical batteries are frequently chosen for this purpose. Lead-acid batteries are one of the most commonly used battery chemistries for these kinds of domestic power systems. Lead-acid batteries are charged using the Constant Current Constant Voltage method (CCCV) [7]. This charging profile starts by applying a constant current to the battery until the terminal voltage rises to a predetermined level; then applying a constant voltage until the input current decreases to zero [7]. Modern chargers implement a third trickle-charge stage that maintains constant voltage in order to keep the battery fully charged to lengthen the life of the battery.

2.4 Maximum Power Point Tracking

A generic off-grid solar-battery system can be seen in Figure 2.

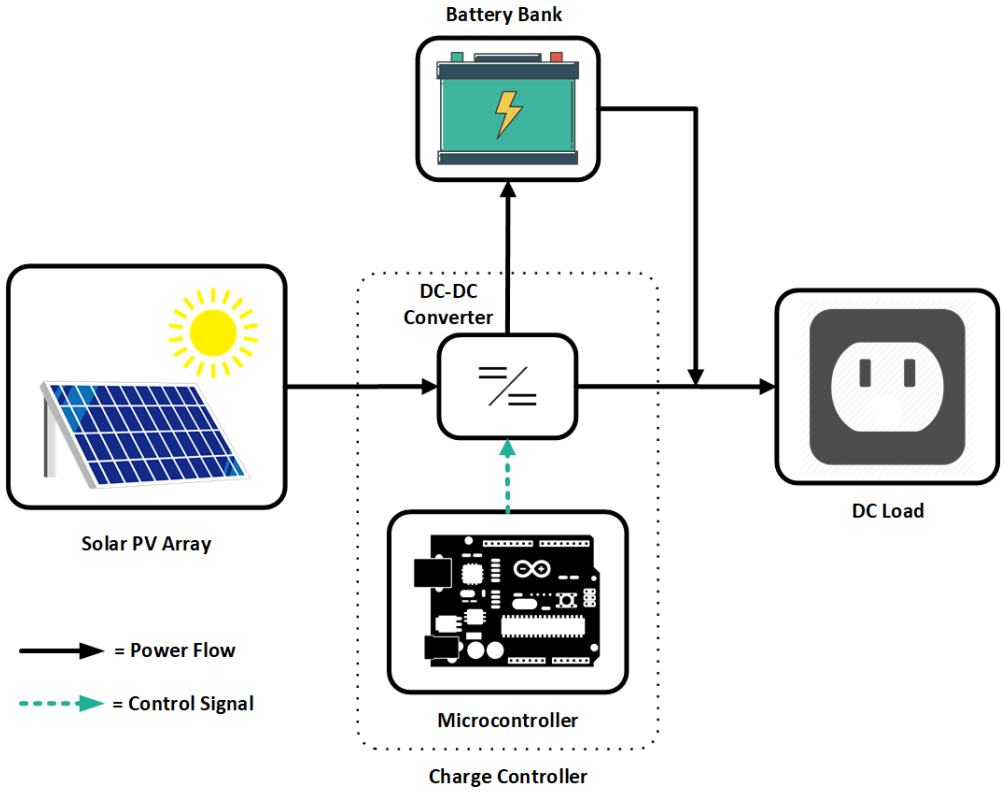

Figure 2: Generic Off-Grid Solar-Battery Power System

The main power source is the solar PV array, from which power flows into the input side of a DC-DC converter. This converter contains power electronic switches that are controlled by pulse-width modulation (PWM) control signals constructed and delivered by a microcontroller. The duty cycle of the control signals determines the ratio of output voltage to input voltage, and in turn allows the charge controller as a whole to maintain the operating point of the panels that yields the most power possible under changing solar irradiance and temperature conditions. The output of the charge controller sends the power produced by the array to the battery bank to conduct charging and also to the load to power appliances. When the battery bank is sufficiently charged and the load is demanding more power than the solar array alone can provide, the battery will discharge in order to meet the demand of the load. [8]

2.4.1 Perturb and Observe Algorithm

The current-voltage (I-V) and power-voltage (P-V) curves for a typical solar panel are seen in Figure 3 below. The intercepts of the I-V curve are the panel's short-circuit current value and its open-circuit voltage value. The panel can only operate at points along this curve. Based on the I-V characteristic curve of the panel, the P-V curve is constructed by multiplying each current value by its corresponding operating voltage and plotting the resultant values versus the voltage axis. On both curves, there is an operating point that yields the maximum power output of the panel under a given irradiance condition. This so-called "maximum power point" can be found at the "knee" of the IV curve and the peak of the PV curve.

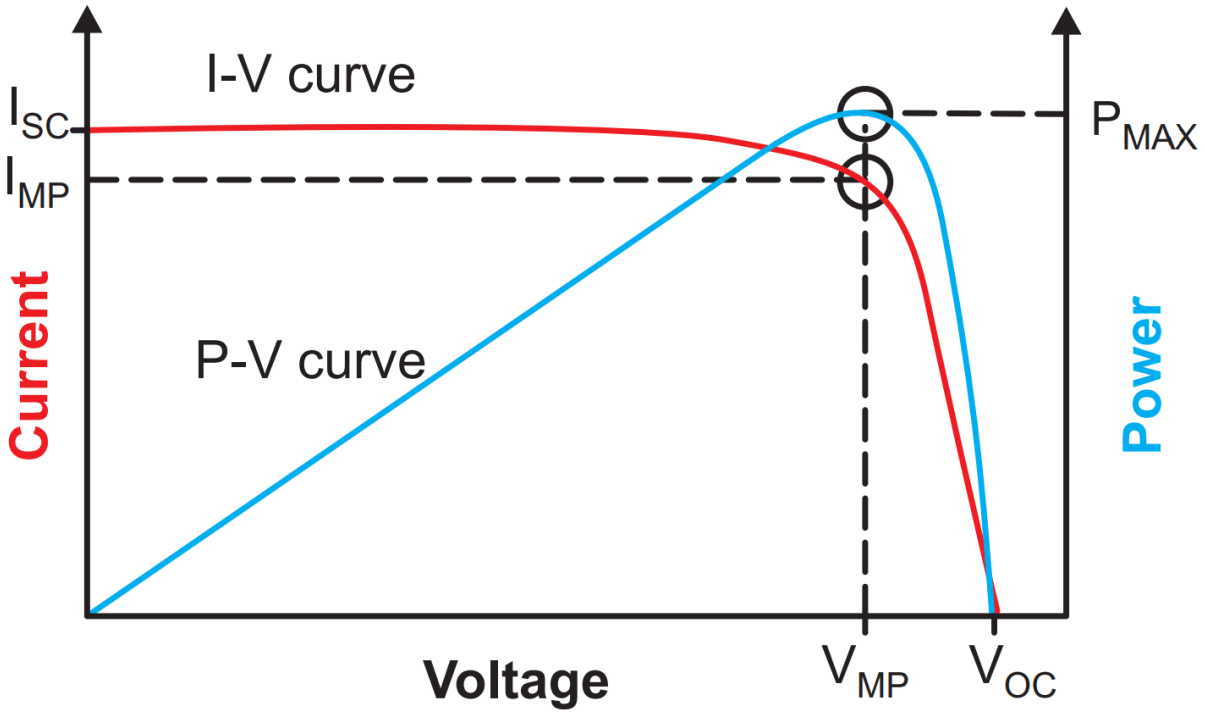

Figure 3: Solar IV and PV Curve [9]

As irradiance levels decrease, the intercepts of the curves shrink in magnitude, and grow in magnitude when solar irradiance increases, all while keeping the curves' general shape. This trend is illustrated by Figure 4, which shows typical I-V and P-V curves at 400 W/m^2, 700 W/m^2, and 1000 W/m^2 of solar irradiance.

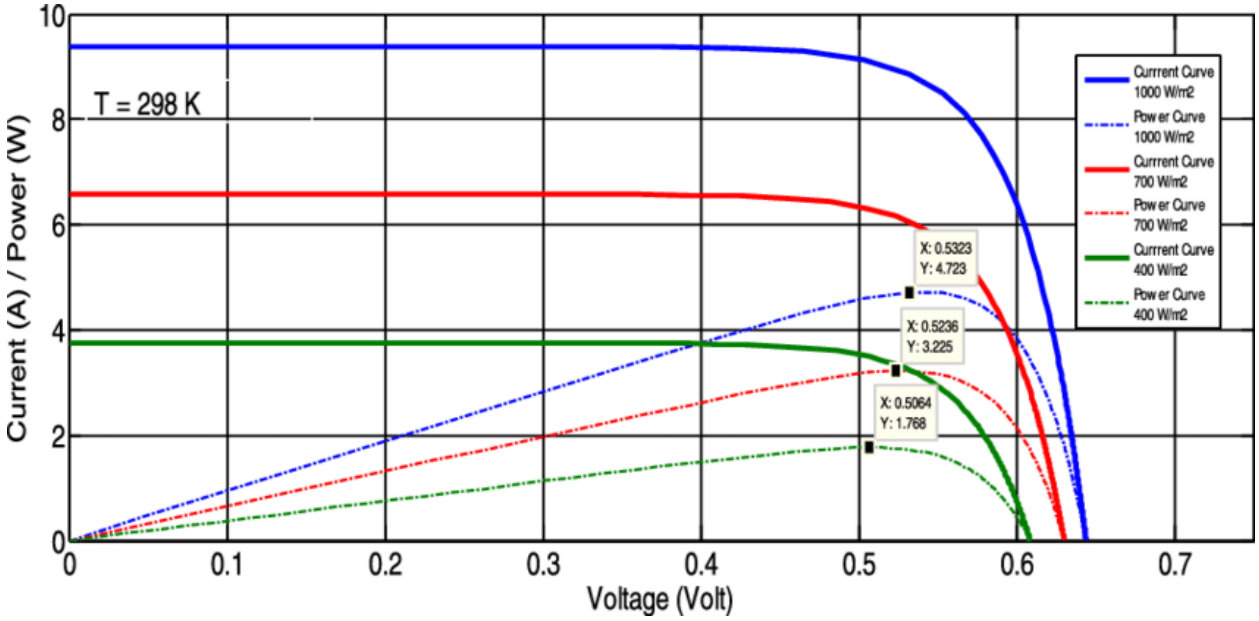

Figure 4: Solar Panel Characteristics Under Varying Irradiance [10]

The main idea behind MPPT is to use a DC-DC converter to adjust the load's impedance from the panel's point of view so that maximum power is extracted for all operating conditions. This is done by acting on the duty cycle of the converter to adjust the operating voltage of the panel(s) on the input side of the converter [11].

In order to "track" the maximum power point of the PV panel(s), a perturb and observe algorithm accepts panel voltage and current measurements as inputs, multiplies the values together to get a power reading, and then evaluates decision blocks that compare the current power value to the previous value as well as the current voltage value to its previous value. The decision blocks and their respective paths are shown in Figure 5.

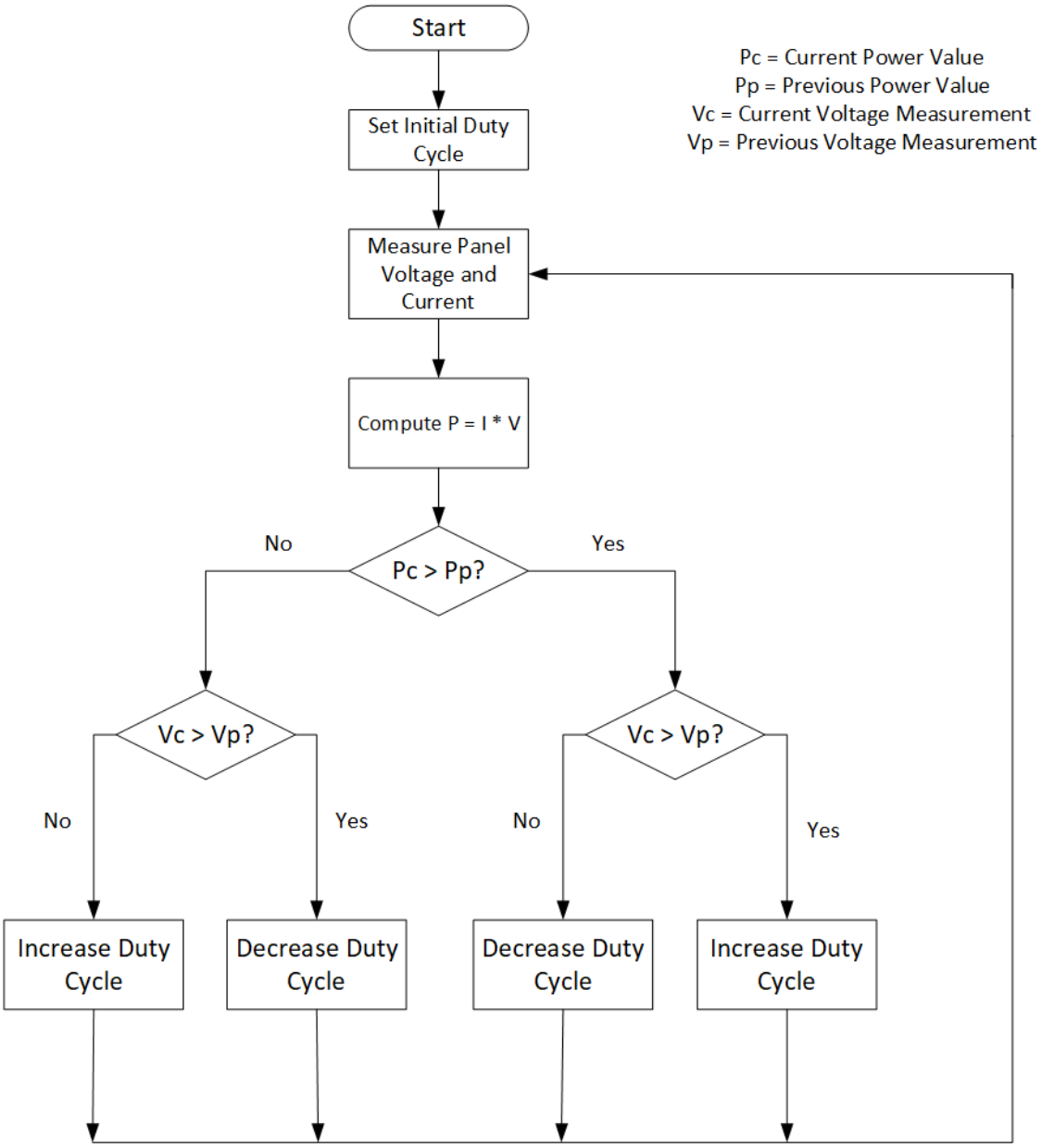

Figure 5: Perturb and Observe MPPT Algorithm

This method can be visualized as a “hill-climbing” algorithm, where the program will start with a given panel voltage along the panel’s P-V curve, then increase that voltage by a given step size, check whether power increased, and decide to increase or decrease the operating voltage of the panel accordingly. If the power increased following an increase in operating voltage, then the algorithm will continue to increase the duty cycle of the converter, and in turn the operating voltage as well. Once the maximum power point voltage is exceeded, the power output will begin to decrease, and the algorithm will decrease the operating voltage by decreasing the duty cycle of the converter. In terms of the hardware implementation of the control signal that varies

the duty cycle, the PWM analog output pins of a microcontroller board are used to send the signal to the gate of the transistor(s) used in the DC-DC converter [12].

The perturb and observe method is not the only type of MPPT algorithm common in practice, and it presents its own advantages and disadvantages compared to other algorithms. Generally speaking, MPPT algorithms can be broken up into two categories, indirect and direct. Perturb and observe is an example of a direct MPPT algorithm because it is constantly taking measurements and performing calculations while in operation. Indirect methods don't take measurements or perform calculations, but rather make simplifying assumptions to operate under instead. Such assumptions are made in the fixed voltage method, where it is assumed that the maximum power point voltage of the panel only changes seasonally, so the converter duty cycle is adjusted less often. The assumption that the panel's maximum power point voltage is a fraction of its open-circuit voltage is made in other common indirect algorithms. These kinds of methods are very simple, but they trade accuracy for that simplicity. Direct methods like perturb and observe are more involved, but often yield greater accuracy on average than their simpler counterparts.

The biggest drawback of the perturb and observe algorithm occurs under rapidly changing irradiance and partial shading conditions. This phenomenon is explored in Figure 6.

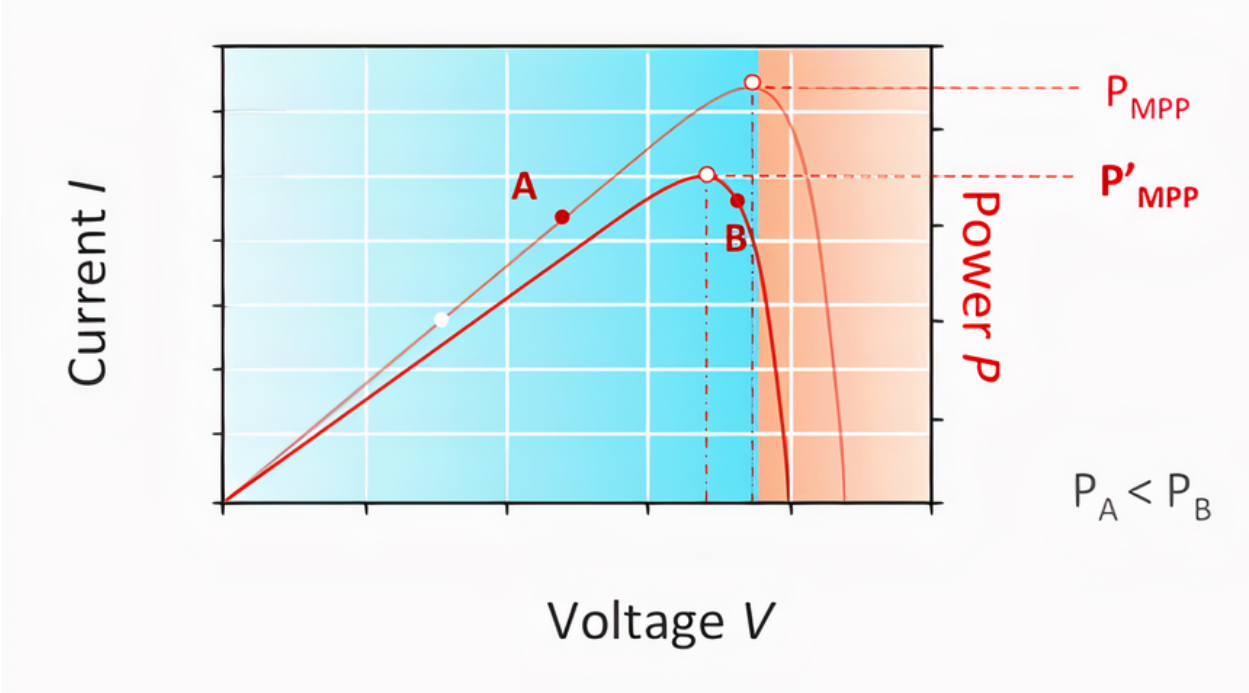

Figure 6: Perturb and Observe Algorithm Drawback [11]

This example starts with an operating point located at point "A". The algorithm decides that the power at point "A" is greater than the previous power value to the left of "A" and increases the

operating voltage to point “B”. At the same time, the irradiance level decreases, shrinking the P-V curve containing “A” to the size of the curve containing “B”, shifting the new maximum power point to the left of the previous maximum power point. Because the power still increased slightly when the algorithm shifted the operating point from “A” to “B”, it will continue to increase the operating voltage by the step size to the right of “B”. The algorithm will then recover upon the next iteration of the loop, after realizing a large power decrease occurred. This extra iteration contributes to unharnessed power that goes to waste [11].

This issue is mitigated by choosing an appropriate step size for your algorithm, taking into account the likelihood of rapidly changing irradiance in the area of system installation. The smaller the step size, the slower the algorithm will converge to the maximum power point, but less likely the algorithm is to waste usable power.

Another issue surrounding the perturb and observe method is partial shading conditions. This occurs when a portion of the solar panel is more shaded than the other regions of the panel. This can be caused by trees or nearby buildings for example. The effect this has on the panel’s P-V curve is that it creates multiple maxima, one or more local and one global. The algorithm can then become stuck oscillating around a local maximum, causing a decrease in efficiency of the system. Some research has illuminated ways to circumvent this issue, with one such project inserting a “checking algorithm” into the basic perturb and observe algorithm that completes a scan of the P-V characteristics of the panel to determine the global maximum power point under partial shading conditions. It then converges to the global maximum and decreases the step size accordingly for optimum steady-state oscillation [13]. This kind of method will be considered as an option for improving the efficiency of our system once we have implemented and tested a basic perturb and observe algorithm and conducted testing to determine the benefits of adding to our algorithm.

2.5 Similar Research

The main inspiration for our chosen system topology comes from a paper titled “Design and Implementation of a Bidirectional DC-DC Converter for Stand-Alone Photovoltaic Systems” published in the International Journal of Computer, Consumer and Control (IJ3C)[14]. In this paper, the authors detail their system topology at a high level and then delve deeper into the hardware design and operation of their bidirectional buck-boost converter, as well as provide test results of their system prototype. Their high-level system diagram can be seen in Figure 7.

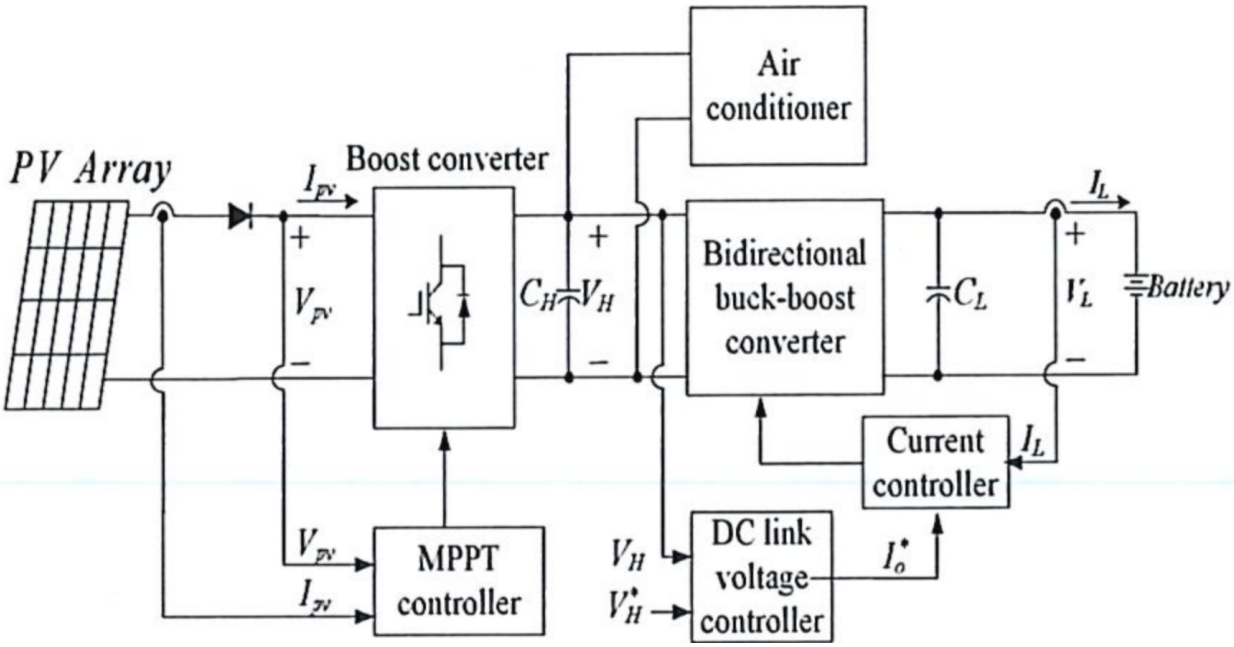

Figure 7: System Framework [14]

The system consists of a PV array and battery bank as power sources, a boost converter controlled by an MPPT algorithm, and a bidirectional buck-boost converter with two levels of control, first, a P-I controller to regulate the load bus voltage (V_H), and second, a hysteresis current controller to adjust and limit the current flowing into and out of the battery. The system is designed to power a small-scale air conditioner as the load. This type of topology appealed to our team because we had run into problems in our previous designs where we needed to be able to control the load bus voltage and the panel operating voltage simultaneously, but were not able to with only one DC-DC converter. Using this design as a reference helped us decide that our design will consist of two converters, one that does MPPT and one that regulates the output voltage.

2.6 Ethical Concerns

With nearly every engineering project comes ethical concerns. As engineers, we must find ways to produce an efficient design while holding the safety and security of the public and the environment in the highest regard, while also keeping moral values at the forefront of the design process. The main concerns surrounding our project involve ensuring safety of those working on this project both this year and in the future, being cognisant of the environmental impacts involved in the manufacturing of our system components, and making sure that we as this year's team in a legacy senior project contribute to the advancement of the project.

Firstly, we have to ensure the safety of those working on the hardware building and testing for this project. In order to avoid electrical faults and injury to team members, we will be making sure that all of our protection elements in our system work correctly. Fuses will be strategically placed throughout the system, and in addition, at the end of this project, we may make a manual that explains to future seniors how to operate or perform tests on the hardware safely, or in the event we keep the hardware, a manual describing how to safely replicate and test projects similar to ours.

Next, we will keep in mind the fact that manufacturing of electrical components can take a toll on the environment, especially in places where raw materials are extracted. Manufacturing plants are large industrial-scale users of electricity, some or all of which comes from fossil-fuel powered plants, which have a large effect on carbon emissions to the atmosphere and contribute to global climate change. The mining and refining processes for raw materials like silicon can also have a considerable environmental impact. Silicon is used to manufacture solar cells, transistors, and microchips, all of which have a place in our system. To refine silicon, high temperature arc furnaces are used to heat silicon-rich sand [15]. These furnaces consume a lot of power to reach such high temperatures and pose a similar problem to manufacturing plants in terms of their electricity source. The mining of silicon deposits in the Earth's crust can also be damaging to various ecosystems and their biodiversity. With these concerns in mind, there isn't a whole lot to be done to avoid them altogether. We can't exclude solar panels from our solar system because of how they are manufactured. Instead, we can only do our best to find ethically sourced and certified manufacturers when shopping for our system components. In addition to that, our system is aimed at giving others access to renewable power where they otherwise would have none, thus leading to a higher quality of life. We believe this purpose aligns well with article I section 1 of the IEEE code of ethics:

> "To hold paramount the safety, health, and welfare of the public, to strive to comply with ethical design and sustainable development practices…" [16]

Lastly, our group must remain aware that this project is a legacy project with a catalogue consisting of two years of other students' work before us. We can't simply copy their work.

Rather, we shall use their work as a guide to help us improve upon their previous designs. We need to stay focused on doing our own work and consulting previous work as a way to confirm or deny our suspicions about a given system problem. Although the system may turn out to be similar to previous years' designs given that the application remains the same, it must remain a product of our group's efforts alone. We can ensure that this happens by doing enough of our own research to have an equal or better understanding than previous students, making all of our own diagrams, simulations, and microcontroller code, and designing our circuit components from scratch, with previous schematics serving only as a reference. All of that being said, it is a legacy project, meaning it is meant to be built upon year after year, so as long as we improve upon last year's efforts, we should be considered a successful legacy project.

2.7 Contribution to Society

This project can contribute to the advancement of engineering and society by serving as a model for similar off-grid solar applications, especially in rural farming communities with no access to power. About 78 percent of the world's poorest people live in rural areas and largely rely on agriculture as their main source of income [17]. 940 million people currently still live without access to power [18]. These are the exact types of communities that an efficient and reliable off grid solar system would be extremely beneficial for.

For many of the almost billion people living without access to power, one must rely on kerosene lanterns for light after dark and wood fuel for cooking [19]. The burning of these polluting fuel sources causes fatal respiratory problems over time, as well as being very carbon emission heavy and contributing to global greenhouse gas emissions. Providing these kinds of communities with reliable access to electricity will greatly improve health, standard of living, economic opportunity, and be beneficial to the climate.

3 Design

3.1 System Diagram

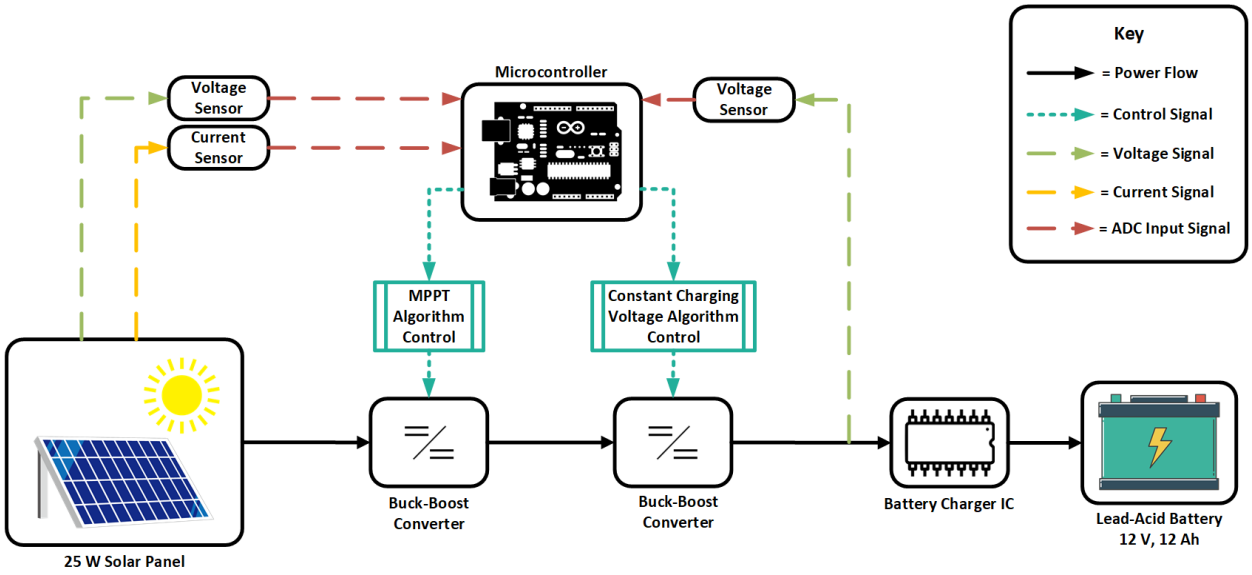

Figure 8: System Diagram

In summary, our system shown in Figure 8 charges a 12 V, 12 Ah lead-acid battery with a 25 W solar panel by controlling power flow through two buck-boost DC-DC converters, the first that regulates the panel operating voltage with a perturb and observe MPPT algorithm and the second, which regulates the input voltage of the battery charging IC to a constant level. The IC then controls the battery charging voltage and current according to a 3-stage charging profile. Voltage and current sensors feed measurement signals into the ADC inputs of an Arduino Microcontroller which manipulates the duty cycle of each converter accordingly.

3.2 MPPT DC-DC Converter

The first custom-made piece of hardware in our system will be a buck-boost DC-DC converter controlled by an MPPT algorithm. The topology and operation of our converter will follow the basic circuit layout described in the background section of this report. One note regarding our implementation is that we will be using a Schottky diode for its low forward voltage drop. To be specific, it should be known that we are using an N-channel MOSFET in our design for its lower "on resistance" compared to a P-Channel MOSFET, and more generally, we are using MOSFETs rather than other controlled switches because of their precise controllability, fast switching, and high current capabilities. Our circuit is seen in Figure 9.

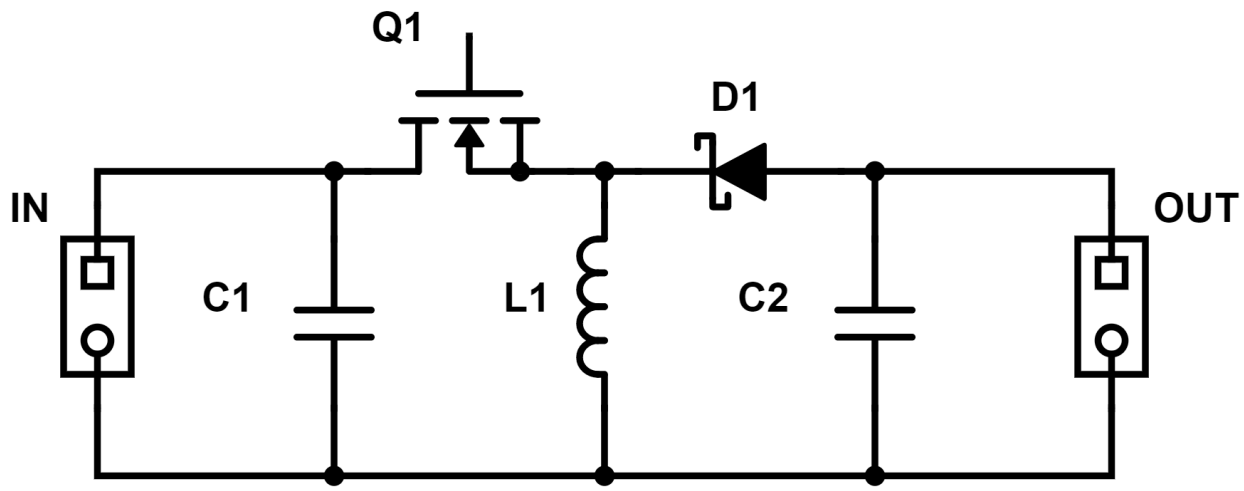

Figure 9: Buck-Boost Converter Schematic

Rather than using an IC for the converter, we wanted to design our circuits from individual components, as the converters are the core electrical design aspect of this project. In terms of calculating the values of the inductors and capacitors in our converters by means of theory, an interesting problem presents itself: Theoretical calculations taught in power electronics textbooks typically apply to the case of an open-loop system with a resistive load. With a dynamic system such as ours, these theoretical calculations can provide a useful amount of intuition regarding tuning the values of the passive components in our circuits, but they don't provide exact values. The key to finding more accurate values is using circuit simulation software that implements numerical solvers to model the dynamic nature of the system. For example, the equations derived in the 4th edition of Power Electronics Devices, Circuits & Applications by Rashid [6] give a great intuition about sizing passive components and choosing switching frequencies:

Peak-to-peak inductor ripple current:

$$\Delta I_L = \frac{V_{in} D}{f_{sw} L} \tag{3}$$

Peak-to-peak output capacitor ripple voltage:

$$\Delta V_C = \frac{I_{out} D}{f_{sw} C} \tag{4}$$

As shown by the equations above, both inductor current ripple and output capacitor voltage ripple depend on the switching frequency and the value of the component itself. Therefore, either an increase in switching frequency or passive component value will lead to a decrease in ripple. Where these equations become less useful is in applications like ours with a dynamic duty cycle and closed-loop control. In our system, the duty cycle has an effect on the input voltage and the

output current as well, which further clouds the usefulness of these formulas in finding exact values. However, in practice, the intuition provided by the theory can help when adjusting component values in a simulation or hardware implementation: Simply increase either the component value or the switching frequency and see what happens to the amount of ripple. This kind of approach will play a much larger role in our simulations and hardware testing than calculating the theoretical values. For example, we are currently limited to a targeted switching frequency of 62.7 kHz for our converter due to the fast PWM capabilities of our Arduino microcontroller, so our only way to decrease voltage or current ripple that we observe will be by increasing our passive component values.

3.3 DC-DC Regulator Converter

In order to charge the battery safely and efficiently, we have decided to regulate the variable MPPT converter output voltage and charge the battery with a TI lead-acid battery charging IC. This second buck-boost converter in our design will require independent and dynamic control logic in order to account for the changing input and load conditions. The control logic will use feedback from the output of the regulator to control its duty cycle. Similar to the MPPT algorithm, this regulator algorithm will track a specified output with a variant duty cycle, but unlike MPPT, this algorithm will be tracking a specified output voltage, not optimizing power output. With this method, our regulator converter will adapt with the changing behavior of the MPPT converter and maintain a constant output voltage. This allows us to power our battery charger IC and in the future, power additional loads.

Currently, we are not ready to implement the regulator converter in hardware. As an early prototype, we plan to simply replicate the MPPT DC-DC converter component values because of the similar ranges at the inputs and outputs. We also intend to research cascaded DC-DC converter stability further after considering the possibility of instability as a result of our independent switching design.

3.4 MOSFET Driver Circuit

To ensure efficient operation of our switching components, we will be using the LTC7000 MOSFET driver IC from Analog Devices [20]. This IC is capable of gate driving MOSFETs at input (drain) voltages between 3.5 V and 135 V and PWM signals between 3.5 V and 15 V. In general, we chose this IC for its wide voltage range, quick transition times, adjustable current limit, protection features and high duty cycle capabilities. This chip is optimized for high-side switching of an NMOS transistor, which is perfect for our design as well. The reference design for the IC is provided in its datasheet and is shown in Figure 10.

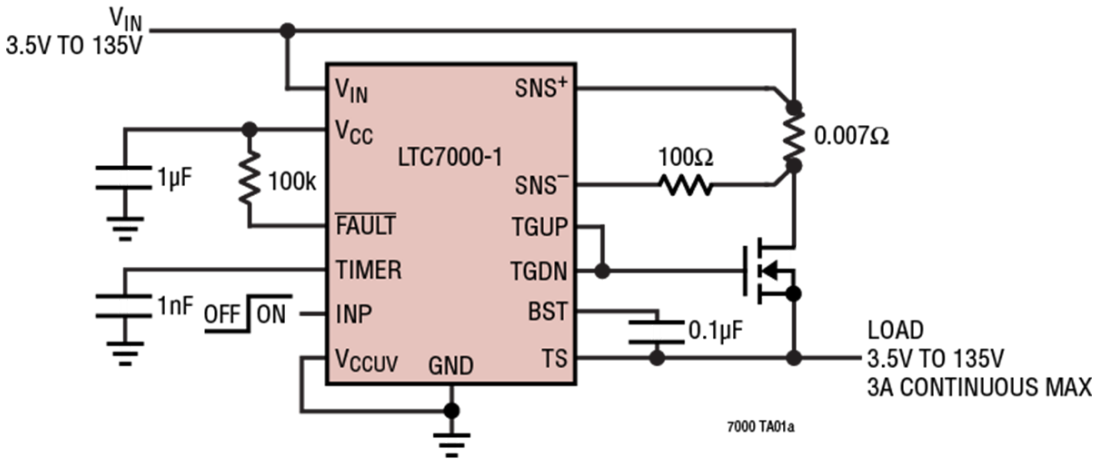

Figure 10: LTC7000 Typical Application Circuit [20]

In our application, V_{in} will be connected to the positive terminal of the solar panel and LOAD will be connected to the node shared by the diode and the inductor in our converters. The PWM control signal from the Arduino will be fed into the INP pin and the TG pins drive the gate of the MOSFETs. We also have the option to leave the SNS pins floating since we are conducting current sensing with a separate module. The full specifications of the LTC7000 can be found in Appendix A.

3.5 Battery Storage And Battery Charging IC Circuit

Our system implements a 12 Ah deep-cycle lead acid battery bank. This battery chemistry was chosen because of its low cost and its well-understood characteristics, which makes it a desirable battery for a testing environment [21]. While our battery bank is much smaller than practical battery banks for off-grid systems, the impedance characteristics of higher capacity banks do not change drastically. For example, the usable capacity and internal resistance of a battery is inversely related to the C-rate, which, given that we are operating our battery below the rated C-rate, it is safe to assume this system is near representative of other systems with the same battery chemistry operating within the same boundaries [22]. This small battery will be adequate for our purposes.

Implementing battery charging requires intelligent voltage and current control based on battery characteristics and active measurements. In order to simplify this portion of our project, we decided that we will implement the TI-BQ24450 Lead Acid Battery Charger IC. This IC contains a state machine and multiple active control loops that detect the battery state of charge and implement CCCV charging [23]. All system parameters are customizable and the circuit design is well explained in the TI-BQ24450 datasheet. Although we are not at a state in our project to have this IC prototyped or integrated in our system, we have begun design considerations.

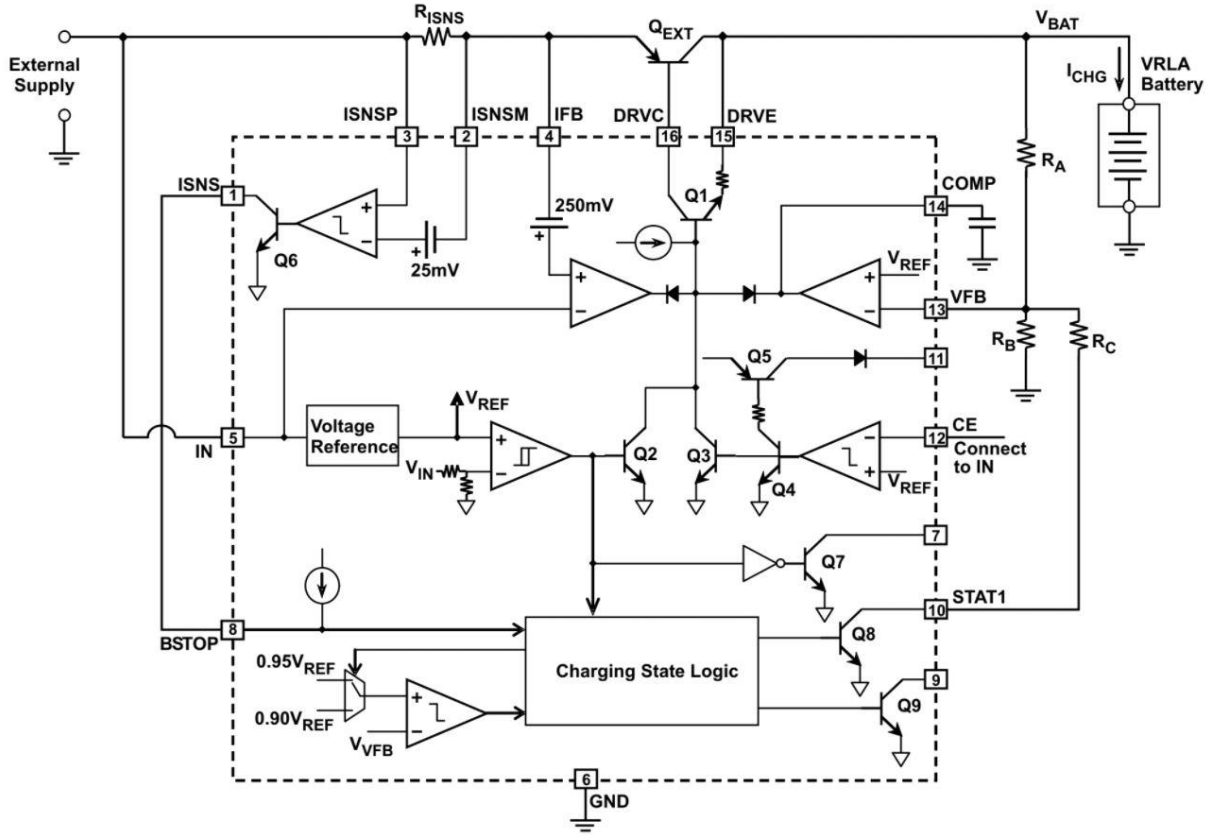

Figure 11: Dual-Level Float-Cum-Boost Charger Application [23]

We plan to use the TI-BQ24450 as a simple dual-level float-cum-boost charger. This allows us to power loads off of the same bus with any excess power [23]. A typical circuit utilizing this topology and the IC block diagram is shown in Figure 11. Assuming we are getting 25 W from our panel, we expect to have a max charge current of about 2 A. We can configure our IC to pass 2 A of charge current with the darlington external transistor topology shown in Figure 12. External passive components are calculated according to the battery characteristics. The data sheet defines V_{BI} as the battery voltage that indicates the end of the constant current stage and the beginning of the constant voltage stage, and I_{TAPER} to be the current which indicates the end of constant current stage and the beginning of the float charge stage. V_{BI} and I_{TAPER} are not yet decided, but their calculations can be found in the data sheet and are as follows:

$$V_{BI} = \frac{0.95 \times V_{REF} \times (R_A + R_B || R_C)}{R_B || R_C} \tag{5}$$

$$I_{TAPER} = \frac{V_{ISNS}}{R_{ISNS}} \tag{6}$$

Where V_{REF} is 2.3 V typical and V_{ISNS} is 250 mV.

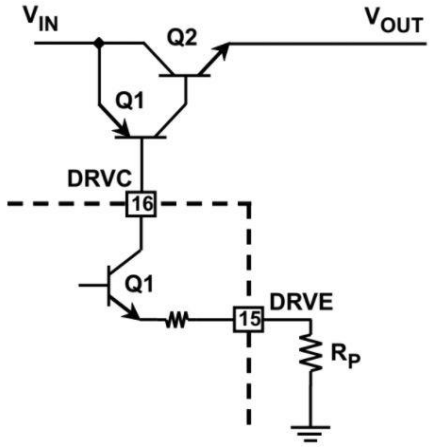

Figure 12: Quasi-Darlington External Transistor Topology [23]

Figure 12 shows the external Darlington transistor topology which allows greater current flow. The TI-BQ24450 datasheet estimates that this topology will allow for charging currents between

0.6 A and 15 A, depending on the transistor. Since we expect 2 A, we decided this topology would be advantageous.

3.6 Control Unit

Our original decision to use an Arduino Uno to execute our MPPT logic was influenced by our familiarity with the Arduino platform and the flexibility of the Uno hardware. Arduino is advertised for PWM applications. However, during our recent prototyping of the MPPT converter, we discovered the default PWM frequency is below 1 kHz. This switching frequency is much too low for practical DC-DC converters, it is uncommon for DC-DC converters to have a switching frequency below 100 kHz, from what we've observed from similar works. This is due to the inverse relationship between switching frequency and ripple on the output voltage and current. Low switching frequencies require very large capacitors and inductors to reduce the output ripple to a usable level.

After investigation, we realized we could increase the Arduino Uno's PWM frequency. In order to increase the PWM frequency we have to reconfigure the timer which is used as the PWM reference signal. After configuration, the timer is capable of outputting a 62.7 kHz PWM signal which, while comparatively slow, we believe will be sufficient for our current and voltage ripple requirements.

Although the full control program has not yet been written for the Arduino, a MATLAB perturb and observe function has been written, tested and shown to be successful in simulation, as has an Arduino program capable of sending a variable duty cycle PWM signal to the gates of our transistors. The code for these programs can be found in Appendices B and C, respectively. In the future, the MATLAB function will be adapted into Arduino code to perform system testing.

Our input signals will be taken from simple voltage and current sensor PCBs. The voltage sensor is a simple linear resistor divider with a heat sink that takes an input up to 25 V and outputs a signal from 0 to 5 V, safe for the Arduino ADC pins. The current sensor is a linear hall effect sensor that accepts 0 to 30 A input and outputs 100 mV/A. We do not expect to have currents higher than 3 A in our system, within standard operation conditions, so our ADC inputs will have to have sufficient sensitivity to the change in voltage.

3.7 Bill of Materials and Cost Considerations

Table 1 describes the components we have ordered for the project, and dictates their unit price, shipping cost, and the total cost. Misc components accounts for electronic components that were previously acquired with unknown costs. The total price for the resistors, inductors, capacitors, diodes, and wiring was estimated.

Table 1: Bill of Materials

Component	Description	Quantity	Unit Price ($)	Shipping ($)	Estimate Subtotal ($)
Solar Panel	Newpowa 25 W	1	36.97	3.14	40.11
Lead Acid Battery	Weize 12V 12Ah	1	24.99	4.29	29.28
Microcontroller	Arduino Uno	1	23.00	7.09	30.09
MOSFET Module	Youngneer-01	2	10.99	0.93	11.92
Voltage Sensors	MH-Electronic	2	9.09	0.75	9.84
Current Sensors	ACS712	2	10.29	0.75	11.04
Battery Charger IC	TI-BQ24450	1	11.98	4.99	16.97
Gate driver IC	LTC7000	1	6.83	7.99	14.82
Misc. components	-	-	10.00	0.99	10.99
Total	-	-	144.14	30.92	175.06

4 Simulation Results

Using a combination of MATLAB Simulink and the PLECS Blockset, our team has simulated several components of our proposed system. This section of the report will focus on the simulations that were functional and yielded meaningful results, as many of them did not.

4.1 Simulation with Resistive Load

First, we constructed a combination Simulink and PLECS model that consists of a solar PV input fed into a buck-boost converter that dissipates power through a resistive load. The converter is controlled by a perturb and observe MPPT algorithm by means of a MATLAB Function block. The duty cycle value from the output of the function is then sent to a pulse generator block to create the switching signal on the gate of the MOSFET in our converter. The model is shown in Figures 13 and 14 below.

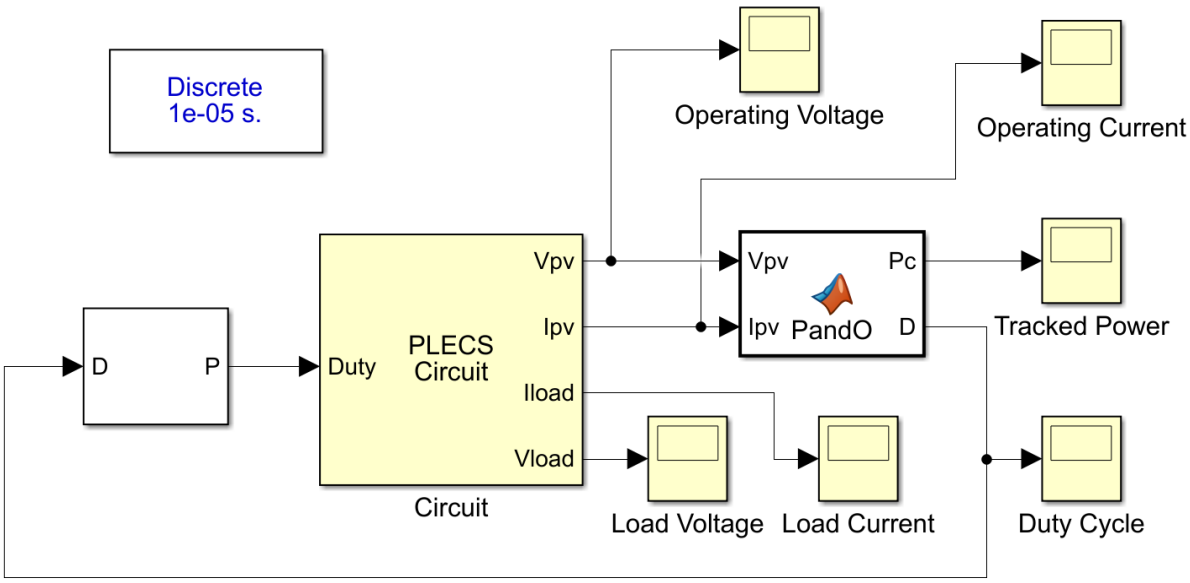

Figure 13: Simulink-Level System Model

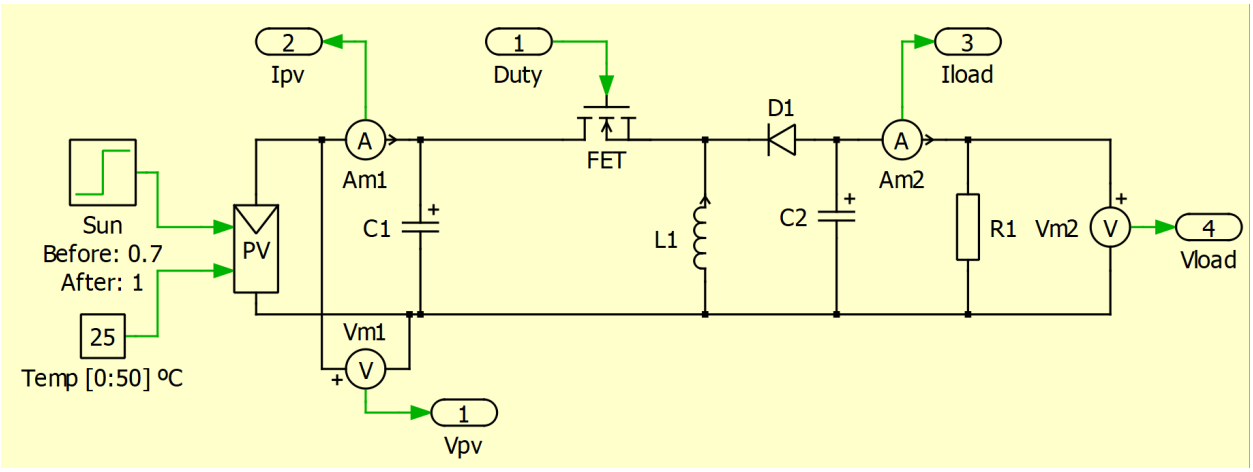

Figure 14: PLECS-Level Buck-Boost Circuit Model with Resistive Load

Parameters: C1 = 500 µF, C2 = 50 µF, L1 = 50 µH, R1 = 200 Ω, V_D = 0 V (Ideal), F_{sw} = 31kHz

The PV module used in this model was developed by Plexim and is based on a BP365 65 W panel from BP Solar [24]. Unfortunately, this was the only model available to us on PLECS and is a higher-powered panel than the one we will be using in our prototype. However, the accuracy and ease of use provided by PLECS makes up for the lack of variety and adjustability. A main purpose of this simulation was to test our MPPT algorithm, and it fulfilled that purpose very well. The panel's maximum power is given as 65 W, with a nominal maximum power point voltage of 17.6 V and current of 3.69 A. The irradiance test function used in the simulation is a step function that occurs at 0.5 seconds, stepping from 700 W/m^2 to 1000 W/m^2 at 25 degrees Celsius (STC).

The MATLAB function that we designed employs a perturb and observe method by taking panel operating voltage and current measurements as parameters, calculates the current power value, and then follows logic that compares the current power value to its previous value in order to decide whether to increase or decrease the duty cycle of the converter. Limits of 15% and 85% are placed on the duty cycle to stay within a safe and efficient range of operation for the MOSFET. The full function can be seen in Appendix B.

The results of the one second-long simulation can be seen below in Figures 15-20.

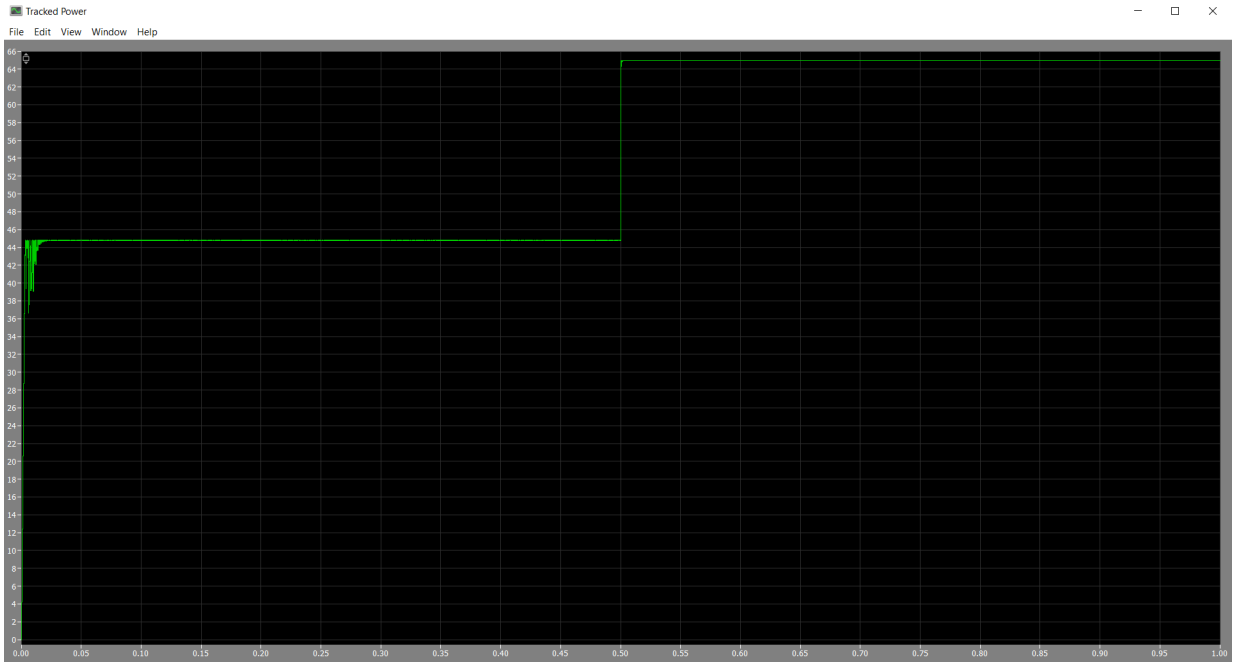

Figure 15: Tracked Power

Starting at the 0.5 second mark, we observed that the known maximum power of the panel, 65 W, is maintained under STC with very little ripple.

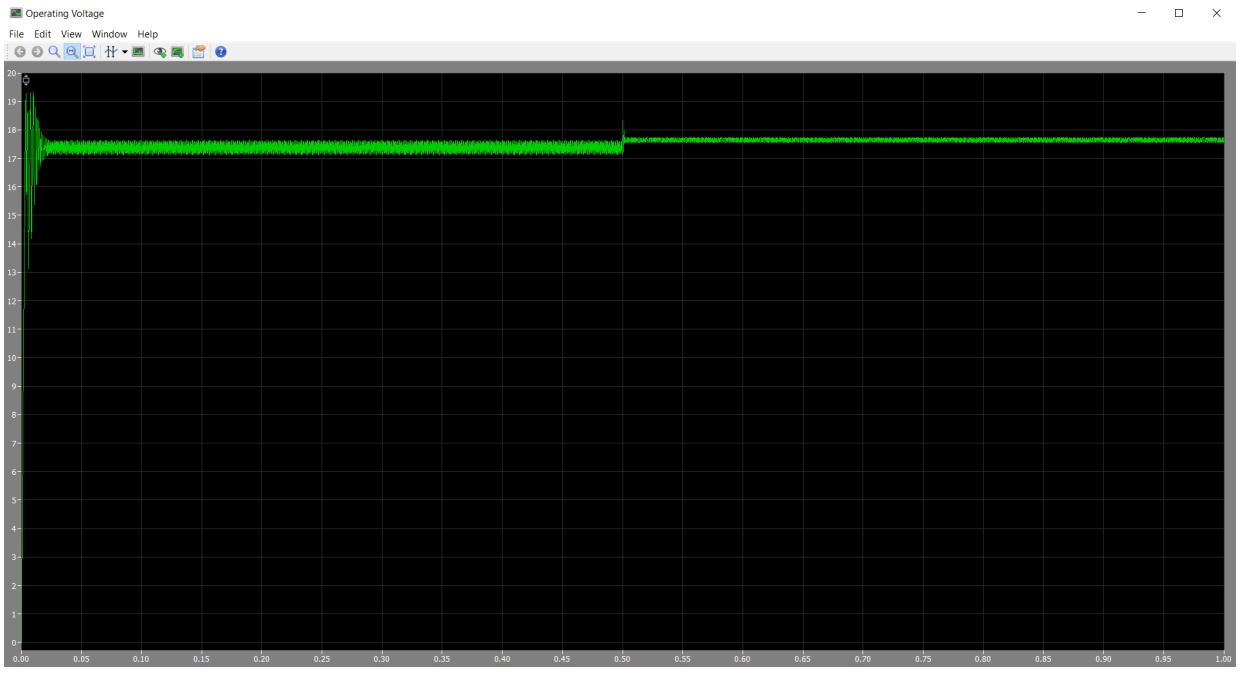

Figure 16: Panel Operating Voltage

As expected, we observed that the operating voltage of the panel increases slightly with irradiance to track the maximum power point, settling at 17.6 V under STC, the nominal maximum power point voltage. The panel voltage ripple also becomes smaller as irradiance increases.

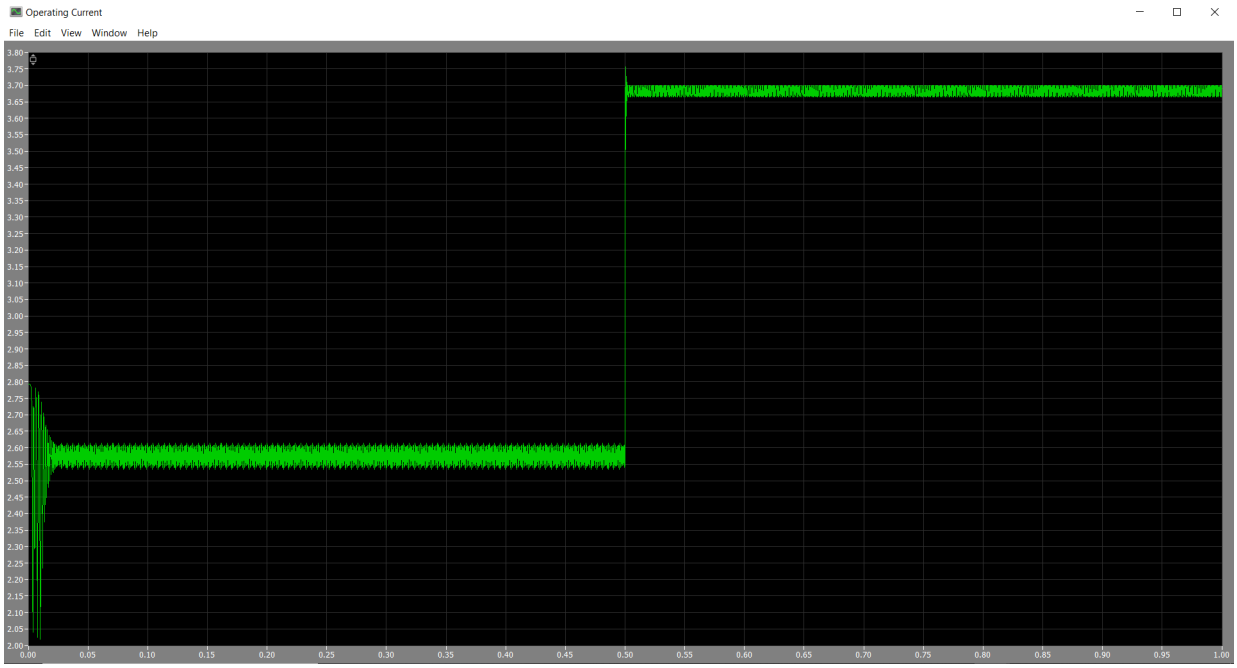

Figure 17: Panel Operating Current

The operating current of the panel increases significantly when irradiance increases, also as expected, and settles around the nominal maximum power current value of 3.69 A.

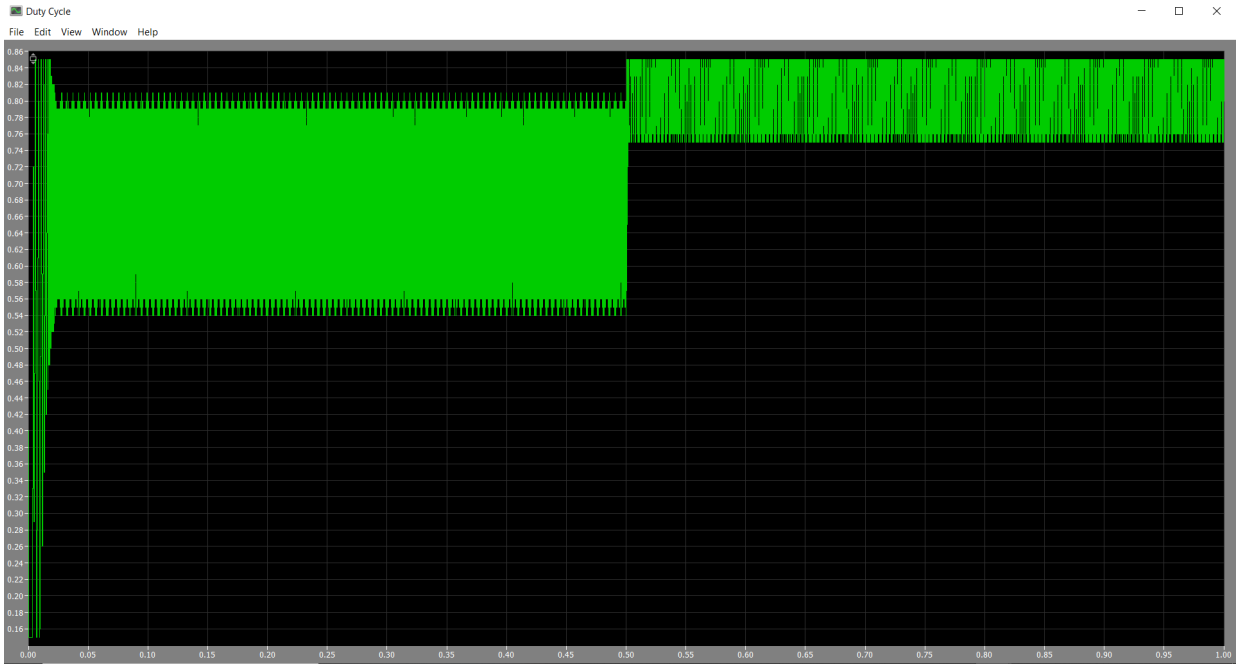

Figure 18: Converter Duty Cycle

The duty cycle increases with irradiance, and varies less. This makes sense because both the panel voltage and current become less variable as irradiance increases.

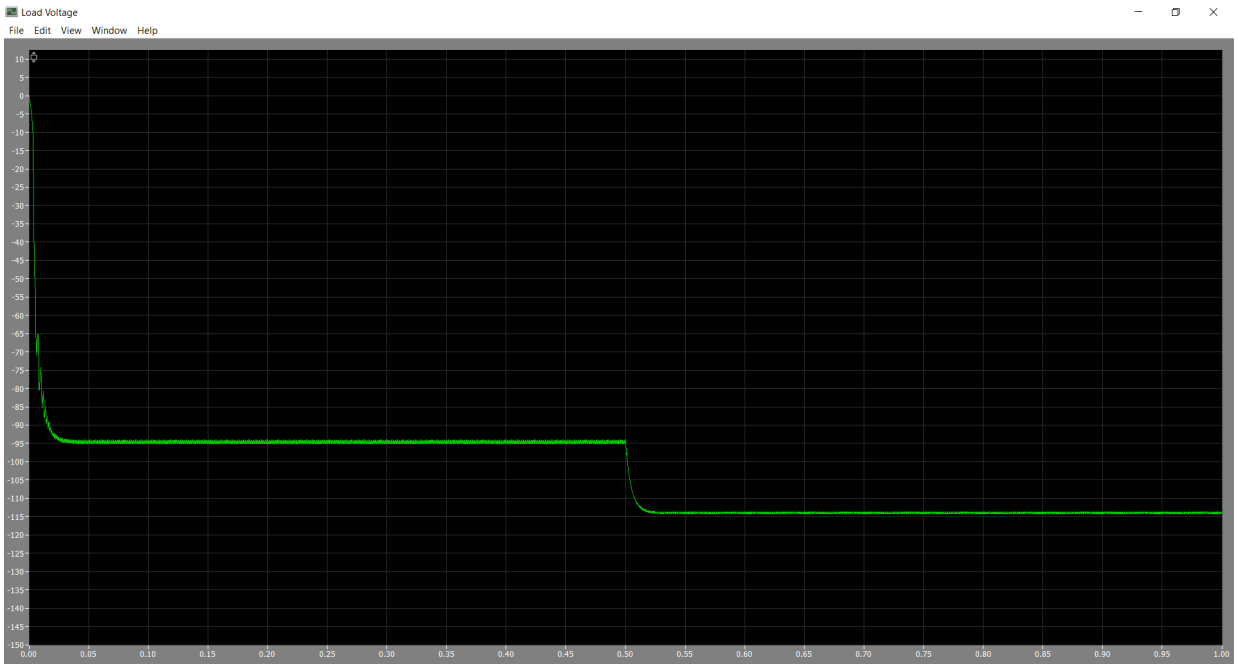

Figure 19: Load Voltage Across 200 Ω Resistor

The load voltage is very high due to the high duty cycle values of the converter. We also observed that the load voltage varies significantly with the resistance of the load. As resistance decreases, so does the load voltage, and the voltage ripple increases.

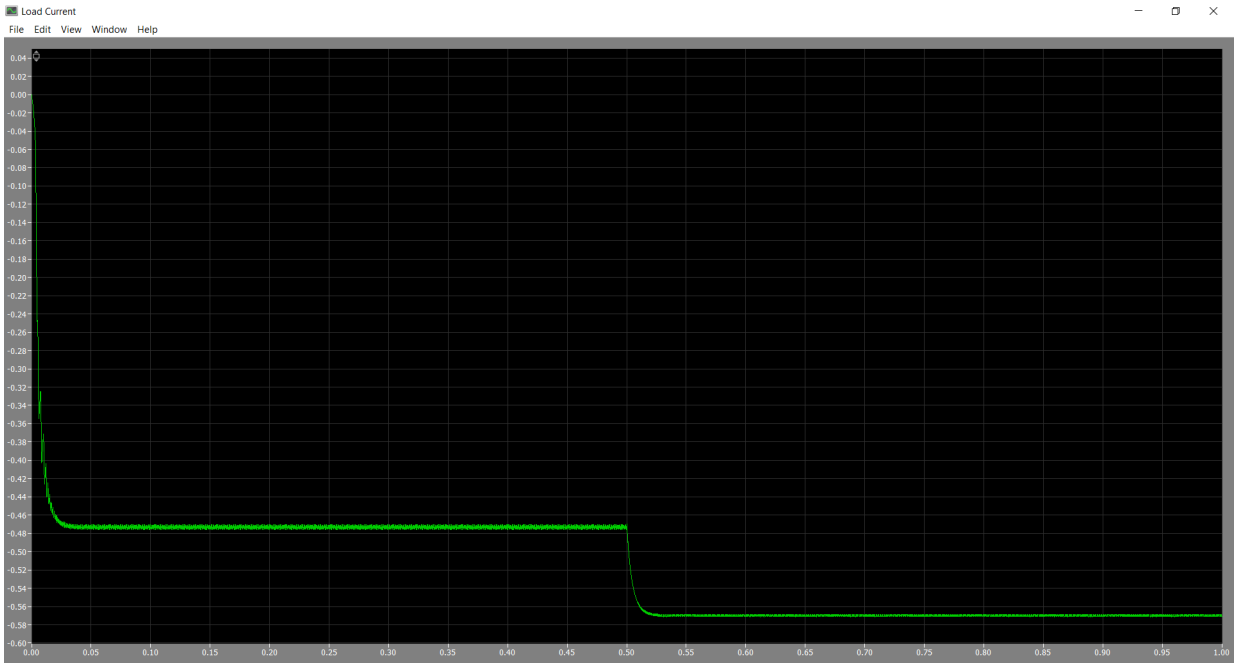

Figure 20: Load Current Through 200 Ω Resistor

Due to the conservation of power, the load current we observed was quite low due to the converter's high duty cycle values and subsequent high load voltage.

We concluded after reviewing these results that the algorithm we have written was controlling the converter effectively and conducting MPPT because the panel was operating at maximum power under STC and the voltage and current were near exactly their nameplate values for maximum power. We also observed the same trends with increasing irradiance that we would expect from an MPPT system. Furthermore, to prove that our converter was conducting MPPT under non-ideal test conditions in addition to STC, we took manual measurements for the PV model to create its I-V and P-V curves under 700 W/m^2 of irradiance. The measurements were taken by isolating the PLECS PV module and connecting resistances from that of a short circuit to that of an open circuit between the panel's terminals. This is demonstrated in Figure 21.

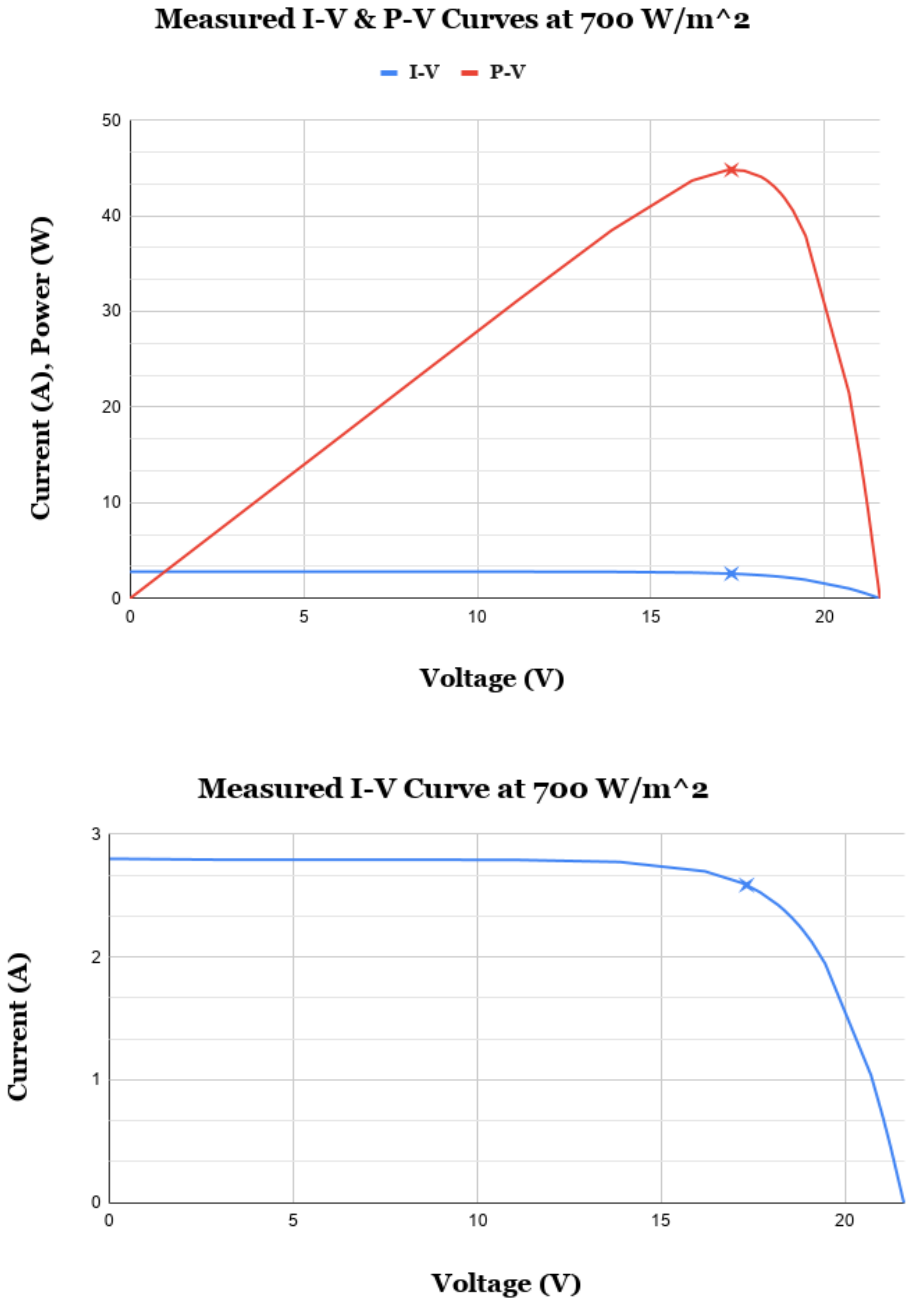

Figure 21: I-V and P-V Curves of Simulated Panel at 700 W/m^2

The P-V curve above shows a maximum power value of 44.791 W (Red 'X' on P-V curve) occurring at an operating point of 17.323 V and 2.586 A (Blue 'X' on I-V curve). Next, we analyzed the resultant power, voltage, and current values from our entire simulation at 700 W/m^2 . Under this irradiance and connected to our MPPT converter, we observed that the panel was outputting 44.78 W at an operating point of 17.39 V and 2.58 A, yielding only a 0.025% error

compared to the measured maximum power value. This allowed us to confidently conclude that our design was capable of conducting MPPT under non-ideal conditions.

4.2 Simulation with Battery Load

Next, we incorporated a battery as the load in our simulation. We used another example model developed by Plexim to do this [25]. The model is of a lithium-ion battery that also outputs the battery state of charge. Although we are using a lead-acid battery in our application, we deemed this model sufficient for our simulation needs because no lead-acid battery model could be found for the PLECS software and this model was able to be adjusted to voltage and capacity values similar to our prototype battery. It is important to note at this point in our hardware testing, it was also determined that we had achieved a higher switching frequency with our Arduino of 62.5 kHz, so this version of the simulation uses a higher switching frequency than the simulation with the resistive load. The model uses the same irradiance signal and perturb and observe control loop as the previous simulation and also runs for one second. The PLECS circuit can be seen below in Figure 22.

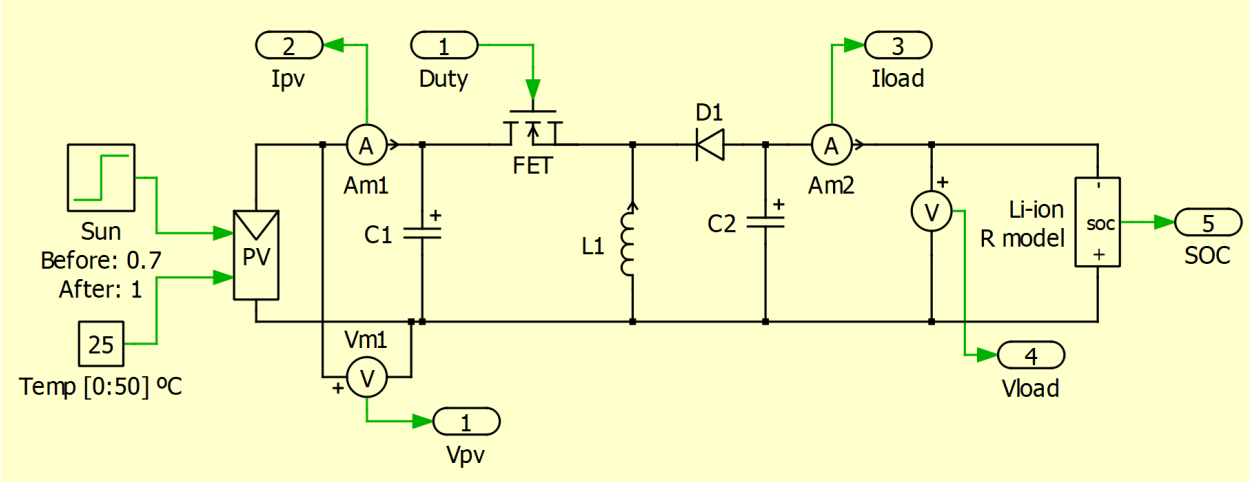

Figure 22: PLECS-Level Buck-Boost Circuit Model with Battery Load

Parameters: C1 = 5 mF, C2 = 5 mF, L1 = 5 mH, Battery: 12 V, 9.6 Ah, V_D = 0 V (Ideal), F_{sw} = 62.5 kHz

One important aspect of this circuit to note is the reverse polarity of the battery. This is done because the output voltage of the buck-boost converter is inverted compared to its input. The capacitor and inductor values were adjusted until optimal performance of MPPT was achieved. The results of the simulation can be seen in Figures 23-27.

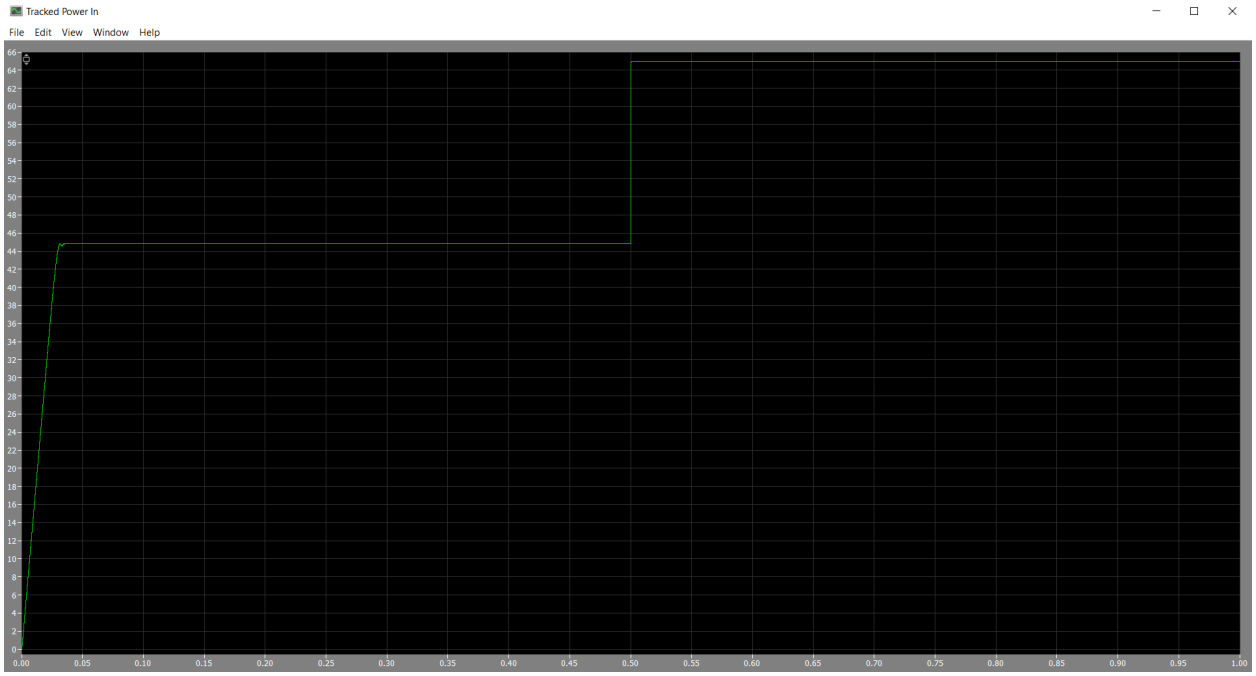

Figure 23: Tracked Power

The system is shown to be tracking the maximum power point very well at both irradiances, with even less ripple, due to the higher switching frequency and larger capacitor values than the previous simulation.

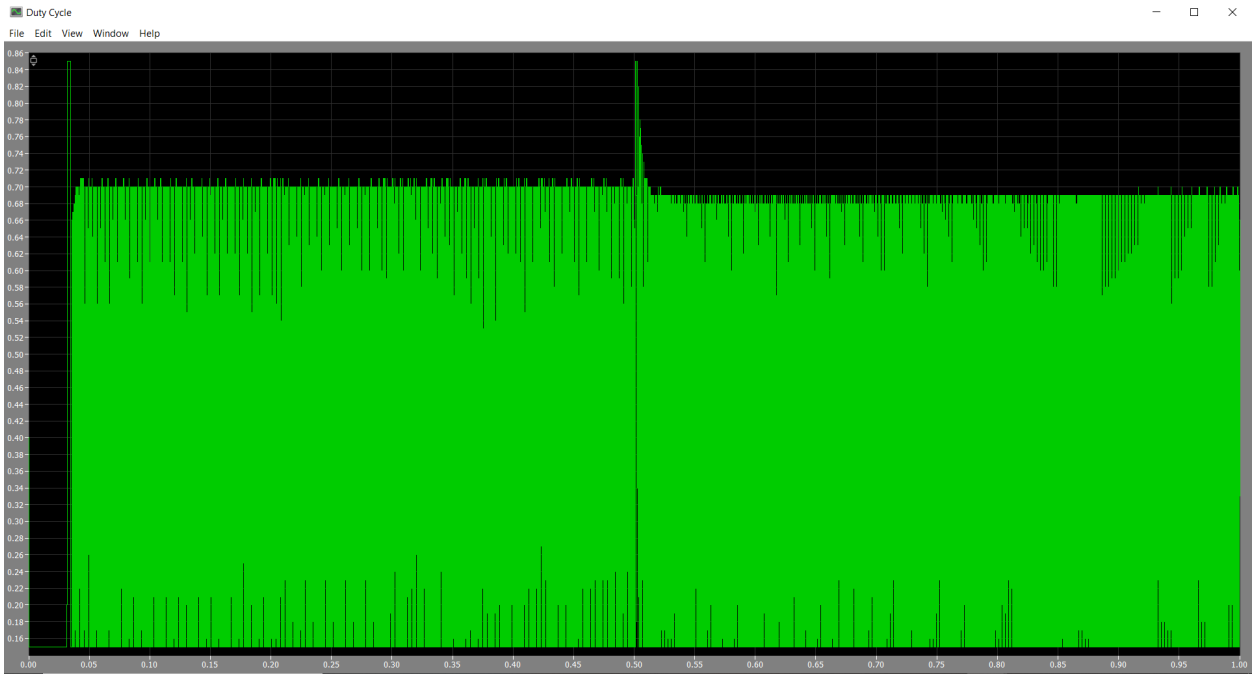

Figure 24: Duty Cycle

The converter duty cycle varies quite a bit and quite quickly in this simulation, from around 15% to 71% for the first irradiance and from 15% to 69% for the STC irradiance level. We hypothesize that this is due to the fact that the MPPT algorithm is sampling extremely fast, at the same rate as the rest of the simulation rather than sampling once every hundredth or thousandth of a second. Our prototype algorithm will not need to sample as fast as this simulation is sampling, so we can assume a less variable duty cycle waveform will be observed when our design is implemented in hardware.

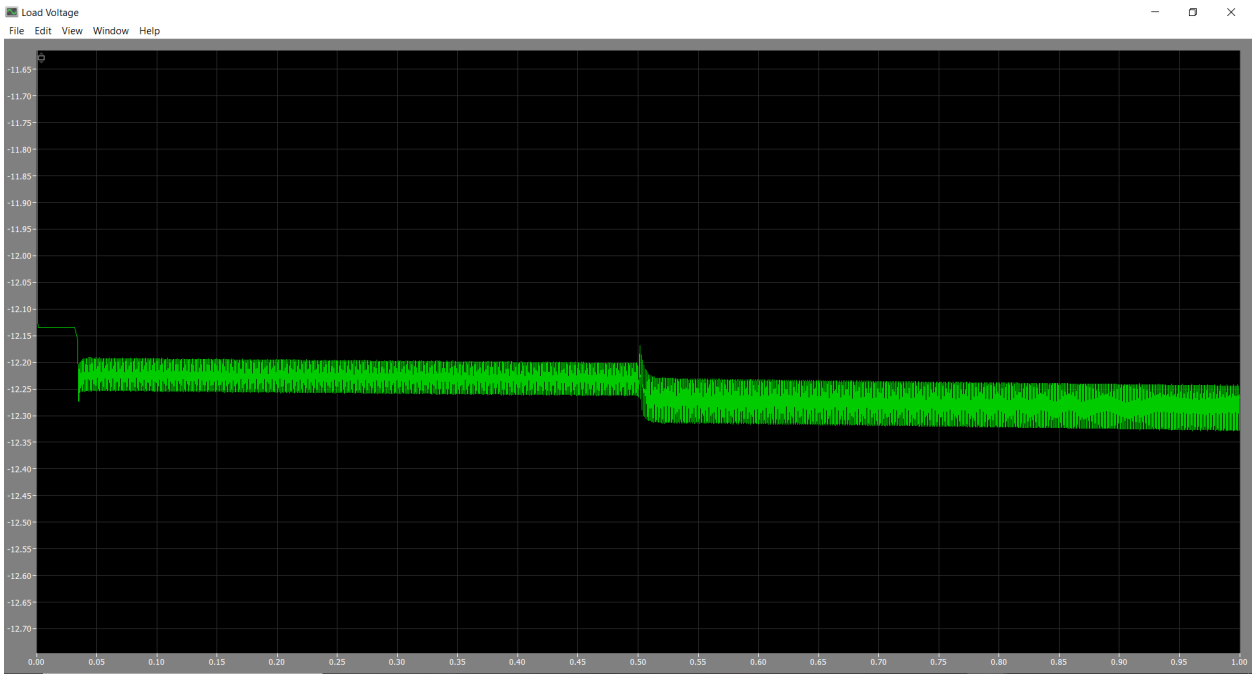

Figure 25: Battery Voltage

The battery voltage steadily climbs over the course of a second while climbing faster under the higher irradiance level as expected. Overall, the main difference between this simulation and the previous one is that the battery “clamps” the output voltage of the converter down to the rated battery voltage of 12 V.

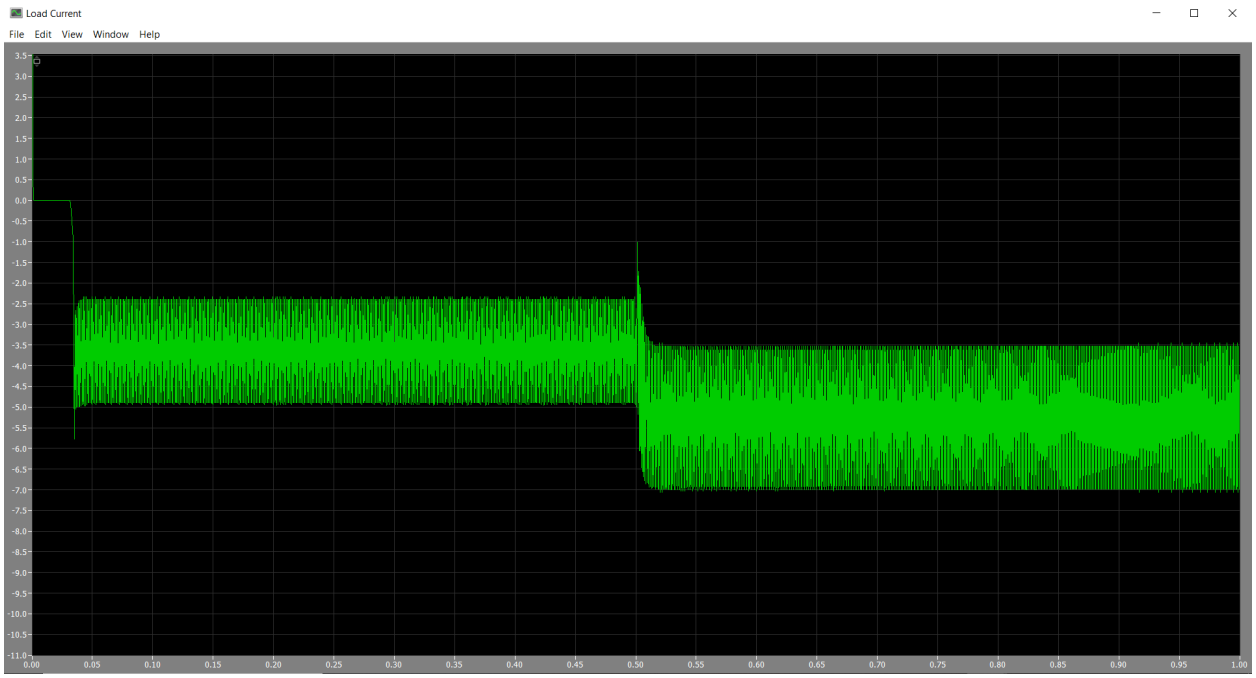

Figure 26: Battery Current

The battery current is relatively high in this simulation, running at about 3.7 A under the lower irradiance and 5.3 A under the STC irradiance level. This is likely due to the fact that the panel used in this simulation is rated at 65 W and is charging a 12 V battery. Conservation of power forces the battery to be charged at those higher current values. In our prototype system, our panel will be much lower power, rated at 25 W, which would yield battery charging currents closer to 2 A maximum.

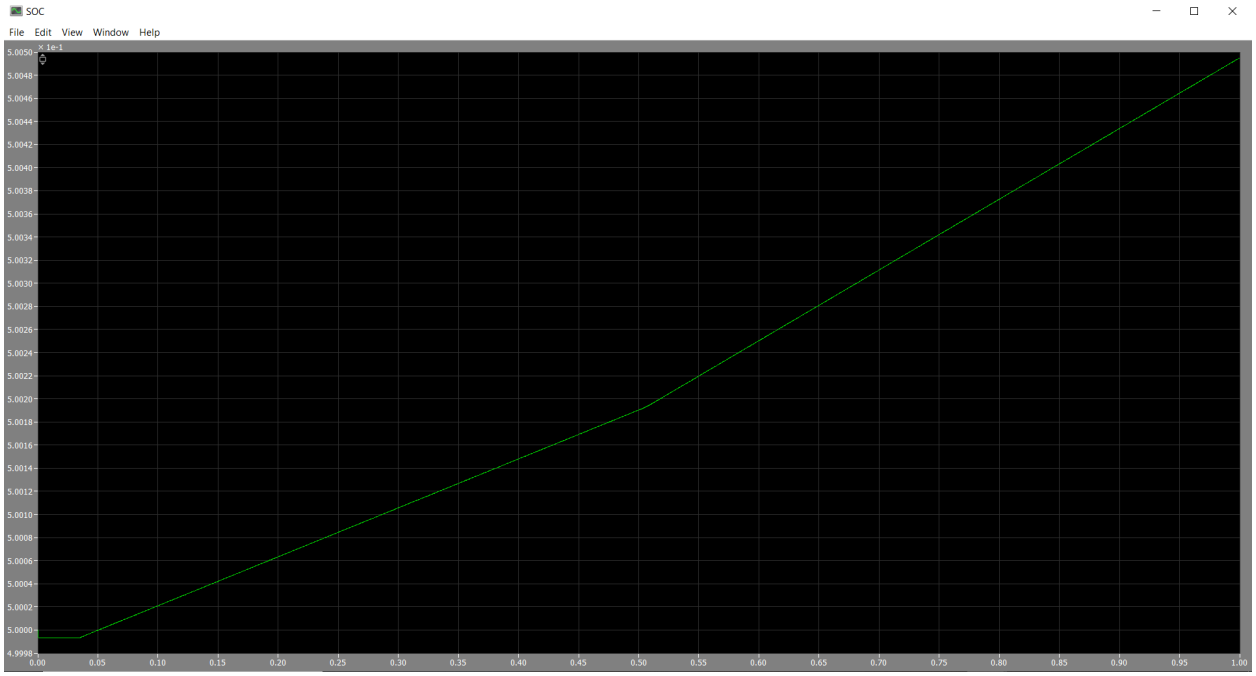

Figure 27: Battery State of Charge

As expected, the battery SOC increased as the system was simulated. The battery started at 50% SOC. With the first irradiance, the battery was being charged at a rate of 0.085% per second and under the STC irradiance, it was being charged faster at 0.1223% per second.

The next step in our simulation process will be to integrate the second converter with its own control loop into the previous simulation. So far, efforts to do this have proved inconclusive, as the simulation runs into “state discontinuity” errors within microseconds of starting. We hypothesized that the independent switching of the two cascaded converters could be causing the discontinuous operation of the system, calling into question the stability of the design. This will become an area of increased research for our team in the coming months and may lead to us adjusting our design to include only one switching component, but implementing additional levels of control in software or in hardware through the use of ICs to ensure safe and stable operation of battery charging.

5 Completed Test Results and Discussion

After simulating the system in MATLAB, we ordered a 25 W solar panel, and acquired basic electronic components, breadboards, a 12 V DC power supply, a digital multimeter, and a basic oscilloscope. Testing was done at home due to the ongoing pandemic. Initial testing of the panels with high power desk lamps produced an open circuit voltage of 15.1 V. The rated open circuit voltage of our panel at STC is 20.23 V, so this value was a fairly close approximation for testing purposes, and allowed us to test under any weather conditions and at any time.

Next, we wanted to test the Arduino's ability to output PWM gate signals to the acquired MOSFET module. To accomplish this, we wrote the code to output a PWM signal from the Arduino and uploaded it to the microcontroller. Appendix C shows the code that sweeps the duty cycle PWM output from 25% to 75%. To test that this was working we took oscilloscope waveforms of the output pins from the Arduino, shown in Figure 28.

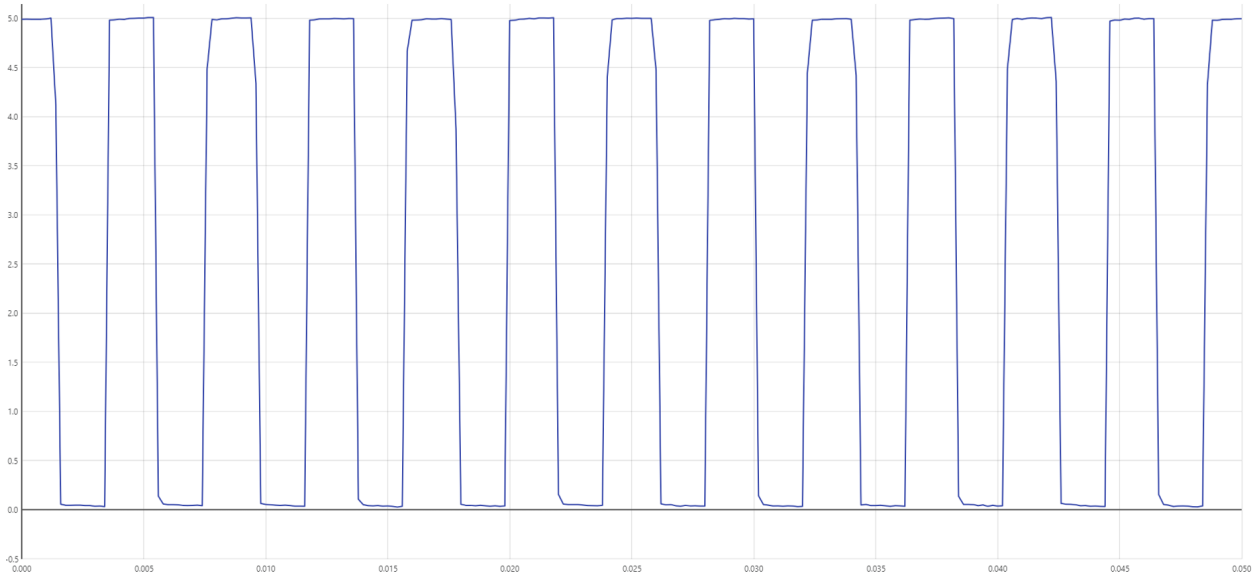

Figure 28: Arduino PWM Signal at ~950 Hz, 50% Duty Cycle

As an additional verification, we wired the transistor module in series with a supply and a small lightbulb. As the duty cycle output was swept across it's range, the lightbulb brightened and dimmed as the average voltage across it varied. This result is shown in Figure 29.

Figure 29: Light Bulb Sweeping Through Brightness Levels with Arduino PWM

Next, the buck-boost converter circuit was physically constructed, Figure 30 shows the buck-boost converter circuit with MOSFET module and power supply input. To test the functionality of the converter, we applied a varying PWM gate signal to the MOSFET module that swept the duty cycle from 0 to 78% of the range of the digital to analog converter. The oscilloscope waveform for that test is shown in Figure 31. It is clear from the waveform that the buck-boost output voltage varies proportionally as the duty cycle is swept.

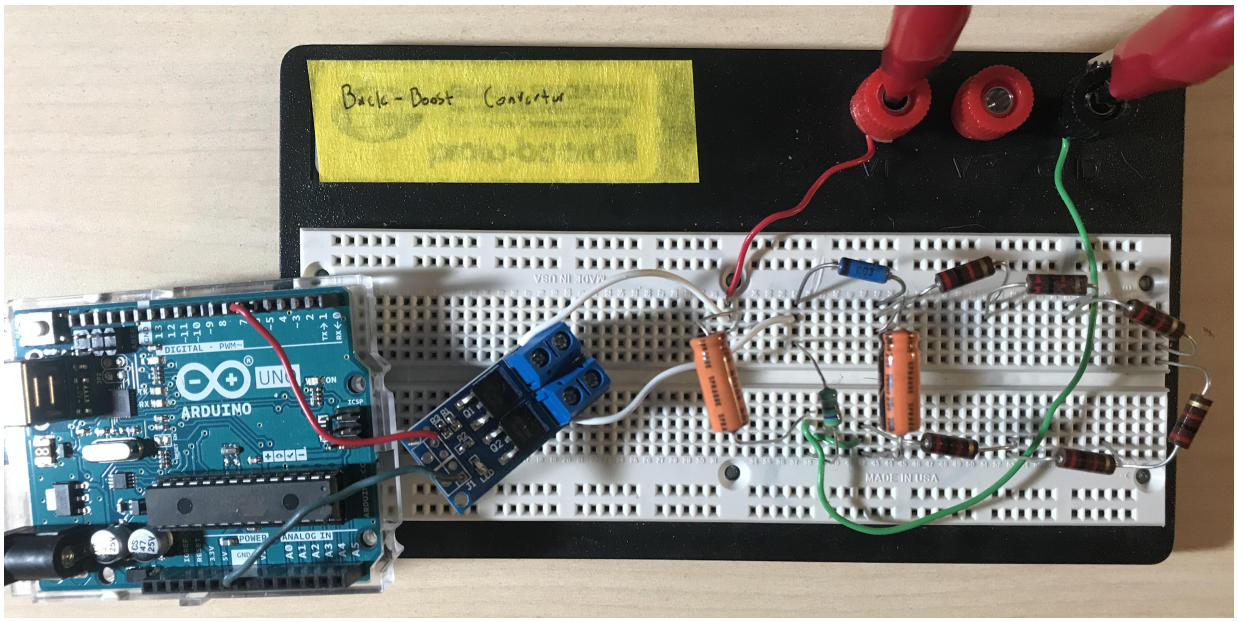

Figure 30: Buck-Boost DC-DC Converter with 12 kΩ Load

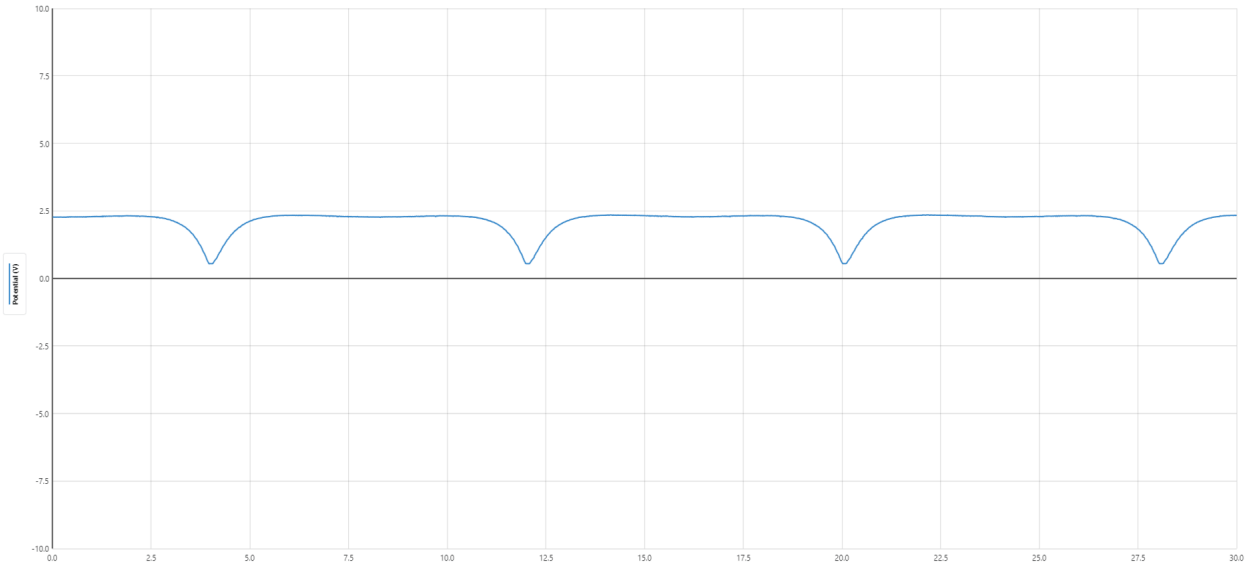

Figure 31: Buck-Boost Output Voltage with 3 V DC Power Supply Input

Next, the 25 W PV panel was connected as the power source and the duty cycle was set at constant values from 10% to 90% with 10% increments to investigate the load and panel voltages as a function of explicit duty cycle. We first took these measurements with the solar panel under a high power desk lamp as the input source. The experimental setup is shown in Figure 32. The results for the solar panel as the input and with the power supply as the input are shown in Figures 33 and 34, with their data tables shown in Appendices D and E. Similarly, Figure 35 shows the panel voltage as the duty cycle varies from 25% to 75%.

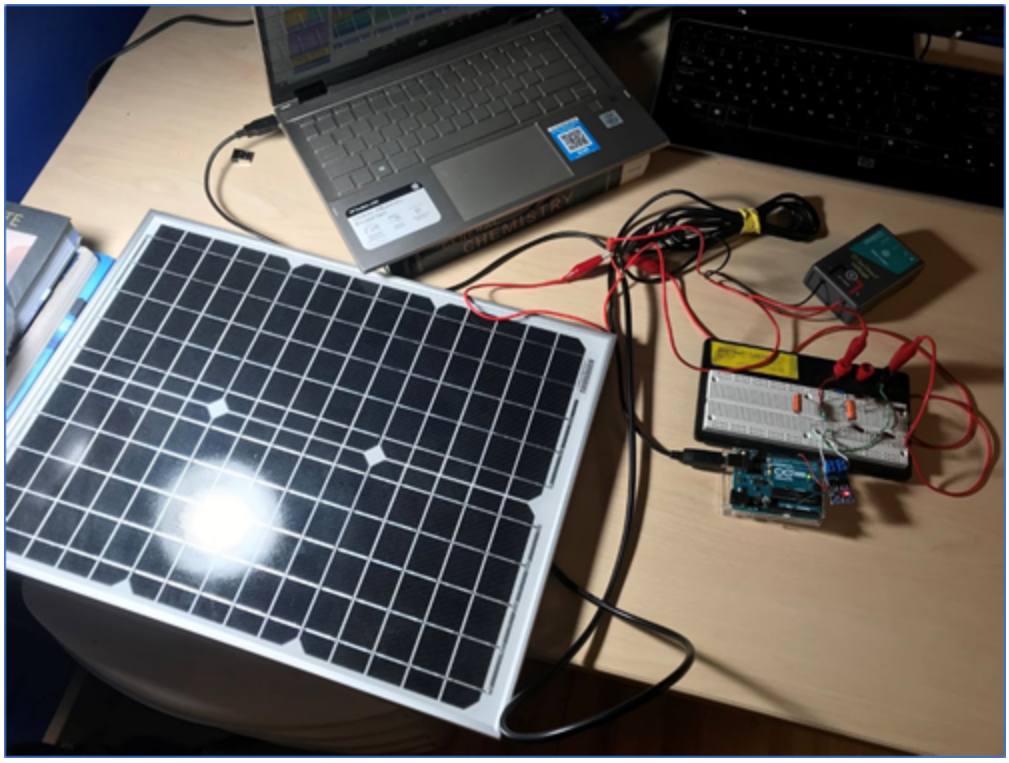

Figure 32: Duty Cycle Testing Experimental Setup

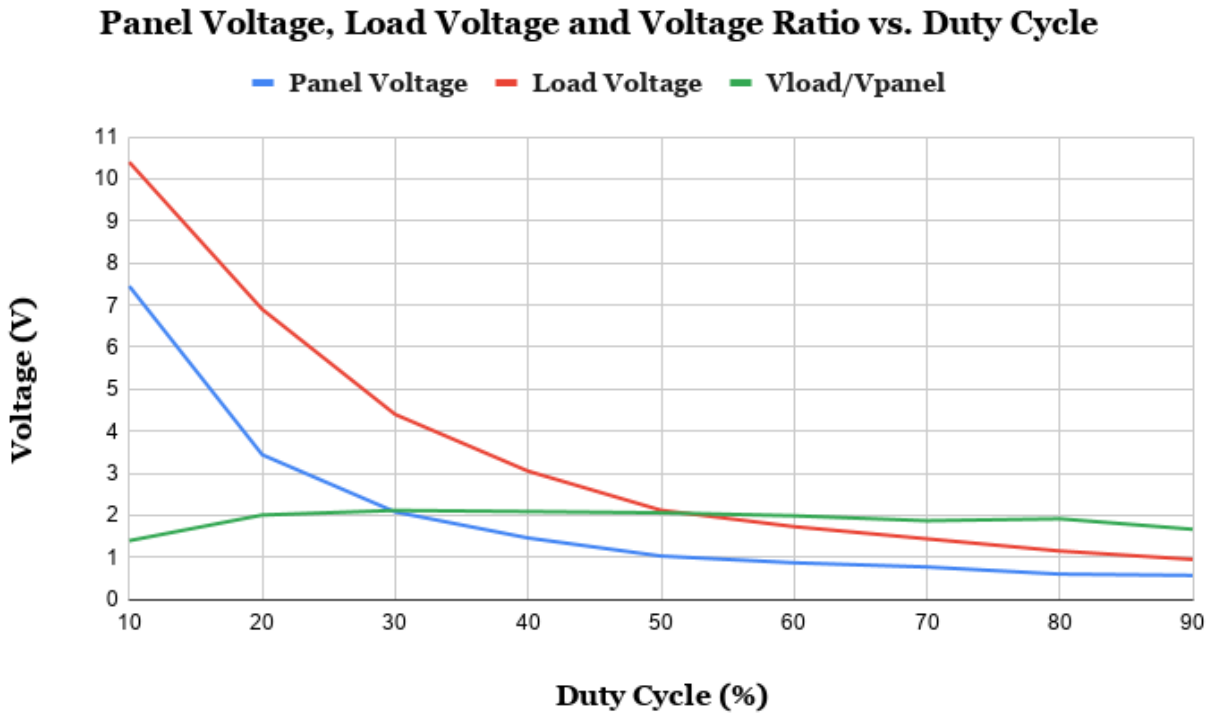

Figure 33: Converter Duty Cycle Testing Results with PV Panel Input

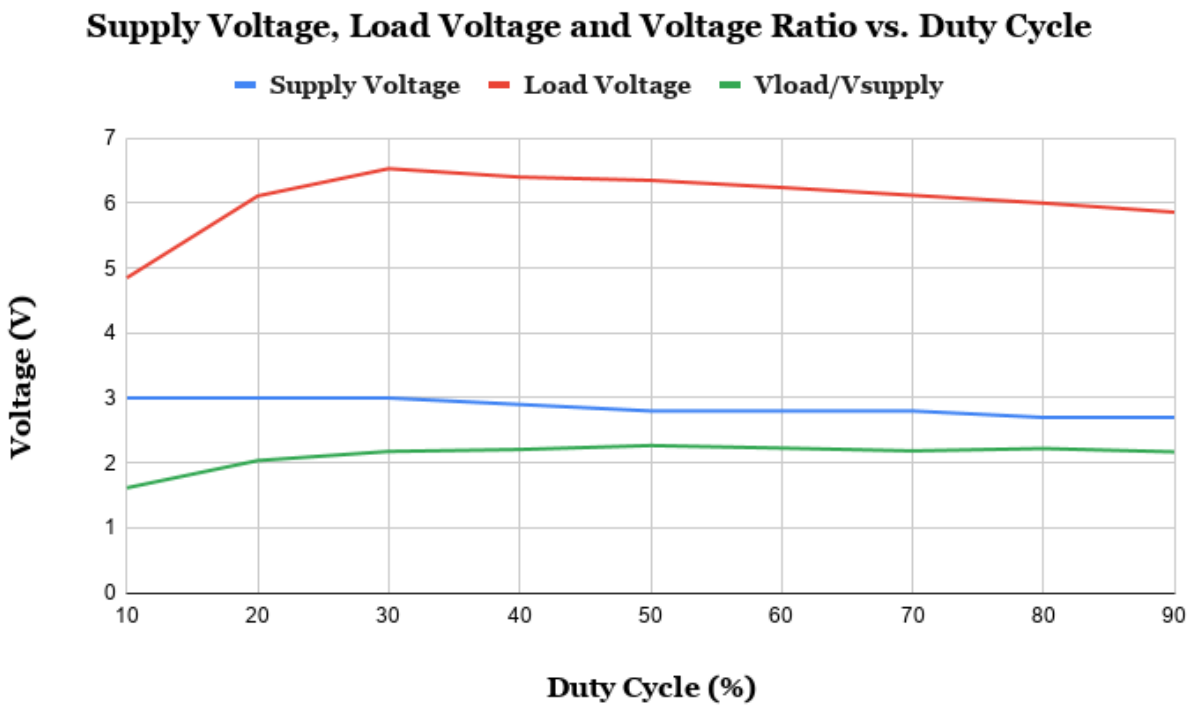

Figure 34: Converter Duty Cycle Testing Results with 3 V Voltage Supply Input

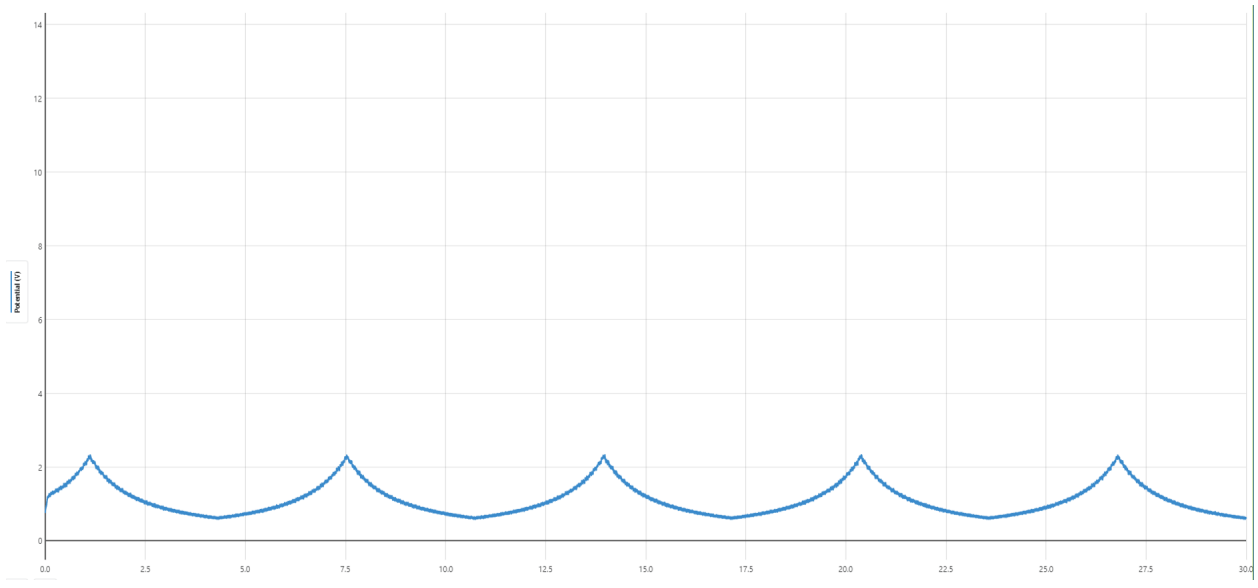

Figure 35: Panel Voltage as Duty Cycle Varies from 25% to 75%

Although it is a good result to verify that we are able to vary the output voltage and regulate the panel voltage as a function of the converter duty cycle, the data we collected did not directly

match the theoretical buck-boost converter duty cycle relationship shown in Equation 2. Our hypothesis for why the theoretical and observed results did not match up is that we were not using a MOSFET driver in our circuit but instead attempting to control the MOSFET directly with the Arduino PWM pin, as the driver IC is currently still in the mail. By implementing this MOSFET driver, along with continuing to fine-tune our component values, we expect the experimental results to match closer to theory. Although we observed a successful fast PWM signal from the Arduino, we weren't able to get successful results in terms of the converter following the theoretical equation even though the switching frequency was significantly higher than in our previous tests. We attribute this result to the lack of a gate driver IC and inaccurate passive component values. We anticipate the converter will work much more efficiently under fast PWM once those two issues are resolved. The verified fast PWM signal can be seen in Figure 36. The duty cycle was verified to be the assigned value from the code of 86% and the frequency achieved is 62.7 kHz, much higher than the Arduino's base PWM frequency of 950 Hz.

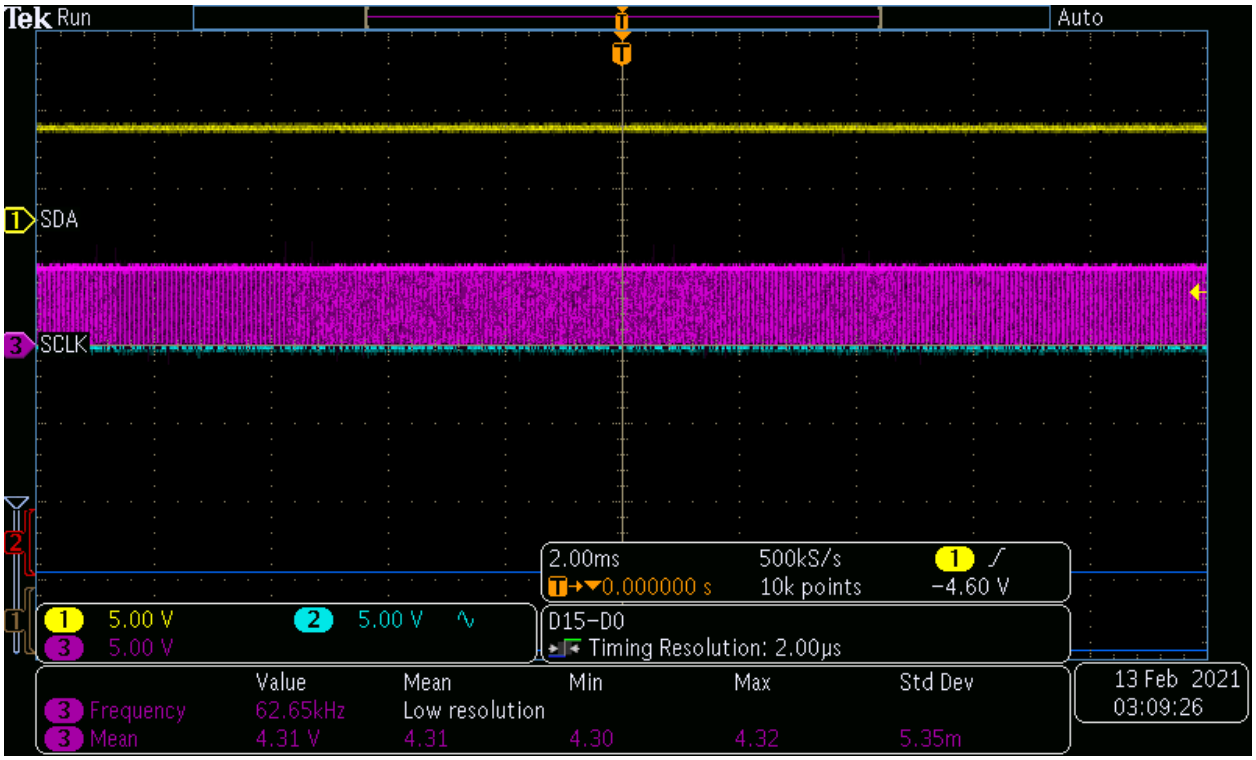

Figure 36: Fast PWM Arduino Output Oscilloscope Waveform at 86% Duty Cycle and 62.7 kHz

6 Future Work

6.1 System Testing Plan

To be able to finish our project in the timeline that we have, a clear plan to test and verify each stage of the system is very important. We have already ordered a MOSFET gate driver module, but are waiting for it to be received in the mail. As soon as it is, we can test our current MPPT stage buck boost converter circuit with a power supply as the input. The output voltage will be tested and compared with the duty cycle set point and the power supply voltage to verify that the converter is following the relationship described in Equation 2. After that, the component values can be varied and tested to find the best setup for this converter stage.

After verifying the MPPT converter stage with a power supply input, the same converter can again be tested with the solar panel as the power source instead of the supply. With a resistive load at the output, the system can be tested to regulate the panel voltage by manually altering the duty cycle, this functionality will be critical to implement the MPPT algorithm. With that working, the voltage and current sensors, along with the code to read them, can be implemented and verified. This can be done by setting up simple resistive circuits with known voltages and currents, implementing the sensors, and guaranteeing that the software readings are correct.

With the converter regulating the panel voltage, and the sensors functional, the MPPT perturb and observe software can be implemented which uses the sensor voltage and current readings to calculate power of the panels and adjust the duty cycle of the converter to maintain maximum power from the panel. This stage can be thoroughly tested under various conditions to ensure that the system is tracking maximum power under different loading conditions and irradiances.

Next, the second, battery stage buck-boost converter can be similarly tested. With the DC power supply as an input, the second converter can be tested to vary the output voltage as a function of duty cycle, again as described in Equation 2. After finalizing the component values, the control software can be implemented, taking the output stage voltage measurement and altering the duty cycle to maintain a constant DC voltage at the output of the converter.

With both converters functional in isolation, the two converters can be cascaded, with the panel at the input and a resistive load at the output. In this way the cascaded system can be verified to simultaneously regulate the panel input voltage to the MPP while also maintaining the constant output voltage that will supply the battery charger IC. The cascaded system can be tested under various operating conditions to ensure functionality under all possible circumstances.

Following this, the battery charger IC can be tested to capably charge the lead acid battery, starting with the DC power supply as the input, then with just the battery stage buck-boost as the

input, and finally the whole integrated system. The full system can then be rigorously tested to verify functionality under a variety of operating conditions.

Finally, an LCD with power, voltage and current measurements could be added as a user interface, and a manual duty cycle control knob could be added to demonstrate the MPPT concept. Additionally, a load could be added at the output to further increase the demonstrational ability, and the breadboarded circuits can be implemented as PCBs for increased form factor.

6.2 Work Schedule

The Gantt chart in Figure 37 describes our expected project timeline from now until the end of spring quarter of our senior year. The objectives section lays out specific tasks to be completed, and the filled in dates outline which weeks we expect to be working on and completing those objectives by. Overlapping objectives means that we will be working on those tasks simultaneously.

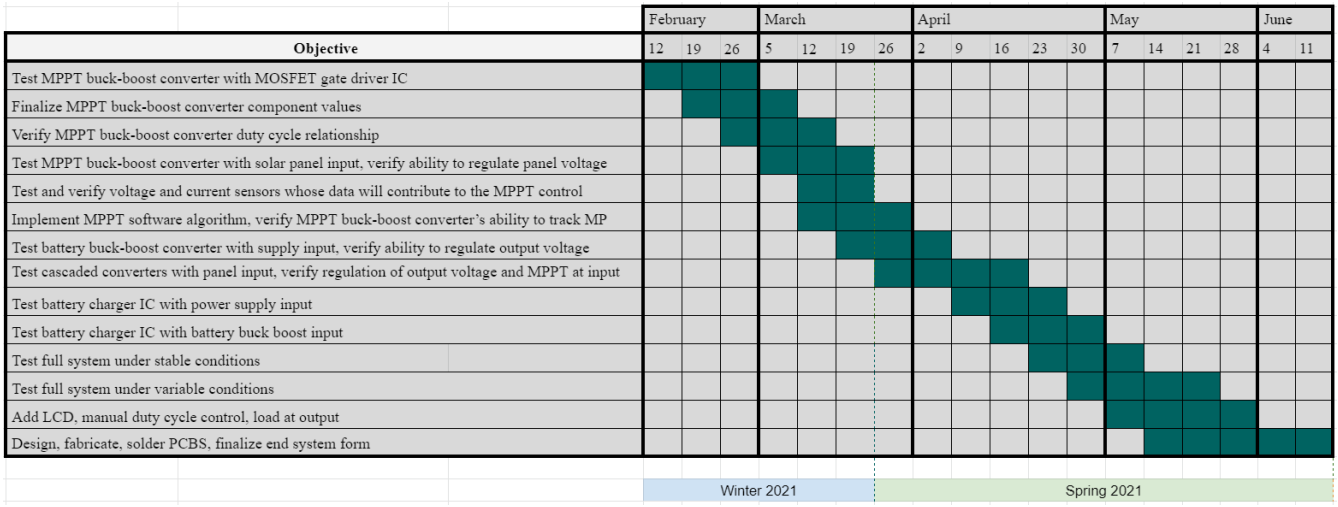

Figure 37: Gantt chart outlining our project timeline from 2/12/2021 to 6/11/2021

6.3 Potential Problems

A potential problem we may encounter and have to find a solution to is the instability caused by the cascading of multiple DC-DC converter stages. Even while each individual stage is stable, the interaction between the stages can be known to cause net system instability. Advanced controller design, like the stability analysis method based on the Floquet theory, can allow guaranteed stability even with the additional dynamics introduced by the integration of multiple converters [26].

7 Works Cited

[1] Li, Dexin, and Pai H. Chou. “Maximizing Efficiency of Solar-Powered Systems by Load Matching.” Proceedings of the 2004 International Symposium on Low Power Electronics and Design - ISLPED 04, 2004, doi:10.1145/1013235.1013280.

[2] Y. Triki, A. Bechouche, H. Seddiki and D. O. Abdeslam, "A Smart Battery Charger Based on a Cascaded Boost-Buck Converter for Photovoltaic Applications," *IECON 2018 - 44th Annual Conference of the IEEE Industrial Electronics Society*, Washington, DC, 2018, pp. 3466-3471, doi: 10.1109/IECON.2018.8591349.

[3] Andrews, John, and Nick Jelley. *Energy Science: Principles, Technologies, and Impacts*. Vol. 3, Oxford University Press, 2017.

[4] U.S. Dept. of Energy. “PV Cells 101: A Primer on the Solar Photovoltaic Cell.” *Energy.gov*, 3 Dec. 2019, www.energy.gov/eere/solar/articles/pv-cells-101-primer-solar-photovoltaic-cell.

[5] Seghers, Nick. *Off-Grid Solar Power Simplified: RVs, Vans, Cabins, Boats and Tiny Homes*. Cleversolarpower.com, 2020.

[6] Rashid, Muhammad H. *Power Electronics: Devices, Circuits, and Applications*. Pearson India Education Services Pvt. Ltd., 2018.

[7] Buchmann, Isidor. “BU-403: Charging Lead Acid.” *Charging Information For Lead Acid Batteries – Battery University*, Nov. 2019, batteryuniversity.com/learn/article/charging_the_lead_acid_battery.

[8] “How Battery Storage Works,” *Khaiyal Solar*. [Online]. Available: http://khaiyalsolar.com/site/index.php/solar-system-2/batteries.

[9] “MPPT Charge Controller Reference Design for 12-V, 24-V and 48-V Solar Panels.” *Texas Instruments*, Texas Instruments, Jan. 2020, www.ti.com/lit/pdf/tiduej8.

[10] Dash, Soubhagya & Nema, Savita & Nema, Rajesh & Verma, Deepak. (2015). A comprehensive assessment of maximum power point tracking techniques under uniform and non-uniform irradiance and its impact on photovoltaic systems: A review. *Journal of Renewable and Sustainable Energy*. 7. 063113. 10.1063/1.4936572.

[11] Smets, Arno, director. *Maximum Power Point Tracking*. *Youtube.com*, Delft University of Technology, 3 Apr. 2019, www.youtube.com/watch?v=5Us5mM87PU8.

[12] J. J. Nedumgatt, K. B. Jayakrishnan, S. Umashankar, D. Vijayakumar and D. P. Kothari, "Perturb and observe MPPT algorithm for solar PV systems-modeling and simulation," 2011 Annual IEEE India Conference, Hyderabad, 2011, pp. 1-6, doi: 10.1109/INDCON.2011.6139513.

[13] R. Alik, A. Jusoh and N. A. Shukri, "An improved perturb and observe checking algorithm MPPT for photovoltaic system under partial shading condition," 2015 IEEE Conference on Energy Conversion (CENCON), Johor Bahru, 2015, pp. 398-402, doi: 10.1109/CENCON.2015.7409577.

[14] Chao, K., et al. *Design and Implementation of a Bidirectional DC-DC Converter for Stand-Alone Photovoltaic Systems*. IJ3C, Vol. 2, No. 3, 2013.

[15] Advameg. “Silicon.” *How Products Are Made*, 2020, www.madehow.com/Volume-6/Silicon.html.

[16] Ieee.org, ”IEEE IEEE Code of Ethics”, 2021. [Online]. Available: http://www.ieee.org/about/corporate/governance/p7-8.html. [Accessed: 02- Feb- 2021].

[17] World Bank Journalism Team. “For Up to 800 Million Rural Poor, a Strong World Bank Commitment to Agriculture.” *World Bank*, 12 Nov. 2014, www.worldbank.org/en/news/feature/2014/11/12/for-up-to-800-million-rural-poor-a-strong-world-bank-commitment-to-agriculture.

[18] Ritchie, Hannah, and Max Roser. “Access to Energy.” Our World in Data, 20 Sept. 2019, ourworldindata.org/energy-access.

[19] Webster, George. “Solar Lamps Replace Toxic Kerosene in Poorest Countries.” *CNN*, Cable News Network, 30 Oct. 2020, www.cnn.com/2012/01/10/tech/innovation/solar-powered-led-lamps/index.html.

[20] Analog Devices. “ LTC7000/LTC7000-1 Fast 150V Protected High Side NMOS Static Switch Driver”. Analog Devices, Mar. 2020, analog.com/media/en/technical-documentation/data-sheets/ltc7000-7000-1.pdf.

[21] Buchmann, Isidor. “Can the Lead-Acid Battery Compete in Modern Times?” *Lead-Acid Rechargeable Battery Information - Battery University*, 2011, batteryuniversity.com/learn/archive/can_the_lead_acid_battery_compete_in_modern_times.

[22] WEIZE. “FP12120 (12V12Ah)”. FP12120. Available: https://m.media-amazon.com/images/I/C1MkyAaT5JS.pdf

[23] Texas Instruments, “Integrated Charge Controller for Lead Acid Batteries”, bq24450. Published April 2009, Rev. Feb. 2012.

[24] Plexim GmbH. “PLECS Demo Model: Single-Phase PV Inverter.” *Plexim.com*, www.plexim.com/sites/default/files/demo_models/single_phase_pv_inverter.pdf.

[25] Plexim GmbH. “Electrical Equivalent Implementation of Lithium-Ion Batteries.” *Plexim.com*, www.plexim.com/sites/default/files/demo_models/single_phase_pv_inverter.pdf.

[26] Li, Hong, et al. “A Stability Analysis Method Based on Floquet Theory for Multi-Stage DC-DC Converters System.” *2017 IEEE Energy Conversion Congress and Exposition (ECCE)*, Cincinnati, OH, 2017, pp. 3025-3029, doi: 10.1109/ECCE.2017.8096554.

8 Appendix

Appendix A: Important Hardware Specifications

LTC 7000 MOSFET Gate Driver

Specification	Value	Units
Input Voltage Range	3.5 - 135 (150 MAX)	V
PWM Input Voltage	-6 - 15	V
Gate Drive Rise Time	13 - 90	ns
Gate Drive Fall Time	13 - 40	ns
Input to Output Propagation Delay	35 - 70	ns

Newpowa Monocrystalline Solar Panel

Specification	Value	Units
Dimensions	$18.11 \times 13.39 \times 0.91$	in
Weight	3.97	lbs
Maximum Power	25	W
Maximum Power Point Voltage	17	V
Maximum Power Point Current	1.47	A
Open Circuit Voltage	20.23	V
Short Circuit Current	1.56	A

* Note: Voltage, Current and Power values listed above correspond to values under STC.

Weize Lead-Acid Battery

Specification	Value	Units
Dimensions	5.94 × 3.86 × 3.74	in
Weight	7.72	lbs
Nominal Voltage	12	V
Capacity (25℃, 20 hr)	12	Ah
Internal Resistance (25℃, Fully Charged)	19	mΩ
Cycle Charging Voltage	14.5 - 14.9	V
Float Charging Voltage	13.6 - 13.8	V
Maximum Charging Current	3.6	A
Maximum Discharge Current (5 sec.)	180	A

AOD4184A N-Channel MOSFET

Specification	Value	Units
Maximum Drain-Source Voltage	40	V
Maximum Gate-Source Voltage	±20	V
Maximum Continuous Drain Current	50	A
Maximum Pulsed Drain Current	120	A
Drain-Source Resistance (On)	<9.5	mΩ
Turn-On Rise Time	17	ns
Turn-Off Fall Time	17	ns

TI-bq24450 Lead-Acid Battery Charger

Specification	Value	Units
Input Voltage	5 - 40	V
Charge Current Range (External Quasi-Darlington)	0.6 - 15	A
Minimum ΔV	1.2	V

Arduino Uno

Specification	Value	Units
Operating Voltage	5	V
Input Voltage	7 - 12	V
Digital PWM Outputs	6	pins
PWM Off - On Voltage	0 - 5	V
Analog Inputs	6	pins
DC Current per I/O Pin	20	mA
Clock Speed	16	MHz

MH-Electronic Voltage Sensor Module

Specification	Value	Units
Output Voltage	0 - 5	V
Input Voltage	0 - 25	V

ACS712 Current Sensor Module

Specification	Value	Units
Current Sensing Range	0 - 30	A
Operating Voltage	5	V
Output Voltage	100	mV/A

Appendix B: Perturb and Observe MATLAB Function

```
function [Pc, D] = PandO(Vpv, Ipv)

% Initialization/Constants
step = 0.01;
Dstart = 0.4;
Dmin = 0.15;
Dmax = 0.85;

persistent Vp Pp Dp;

if isempty(Vp)
    Vp = 0;
    Pp = 0;
    Dp = Dstart;
end

Pc = Vpv * Ipv;
Vc = Vpv;
D = Dstart;

if (Pc > Pp)
   if (Vc > Vp)
       D = Dp - step;
   elseif (Vc < Vp)
       D = Dp + step;
   elseif(Vc == Vp)
       D = Dp;
   end
elseif (Vc > Vp)
    D = Dp + step;
elseif (Vc < Vp)
    D = Dp - step;
elseif (Vc == Vp)
    D = Dp;
end

if (D < Dmin)
    D = Dmin;
```

```
end

if (D > Dmax)
    D = Dmax;
end

Vp = Vc;
Pp = Pc;
Dp = D;

end
```

Appendix C: Arduino Code for Duty Cycle Sweep

```
int pwmPin = 6; // pin to connect to MOSFET module
int Duty = 64; // variable to hold duty cycle value
int Step = 4; // increment/decrement step for PWM duty cycle

void setup() {

  pinMode(pwmPin,OUTPUT); // set pwmPin as output
  Serial.begin(9600);

}

void loop() {

analogWrite(pwmPin, Duty); // send duty cycle value to MOSFET
  Duty = Duty + Step;

  if (Duty <= 64 || Duty >= 192) {
    Step = -Step;
  }

delay(500);

}
```

Appendix D: Converter Duty Cycle Testing Results with PV Panel Input

Duty Cycle	Arduino DAC Value	Panel Voltage	Load Voltage
10%	26	7.45	10.40
20%	51	3.44	6.90
30%	77	2.08	4.40
40%	102	1.46	3.05
50%	128	1.03	2.12
60%	153	0.87	1.73
70%	179	0.77	1.44
80%	204	0.60	1.15
90%	230	0.57	0.95

Appendix E: Converter Duty Cycle Testing Results with 3 V Voltage Supply Input

Duty Cycle	Arduino DAC Value	Supply Voltage	Load Voltage
10%	26	3.0	4.85
20%	51	3.0	6.11
30%	77	3.0	6.53
40%	102	2.9	6.40
50%	128	2.8	6.35
60%	153	2.8	6.24
70%	179	2.8	6.12
80%	204	2.7	6.00
90%	230	2.7	5.86